

The effects of Antarctic alteration and sample heterogeneity on Sm-Nd and Lu-Hf systematics in H chondrites

Maeda, Ryoga; Goderis, Steven; Debaille, Vinciane; Pourkhorsandi, Hamed; Hublet, Geneviève; Claeys, Philippe

Published in:
Geochimica et Cosmochimica Acta

DOI:
[10.1016/j.gca.2021.05.005](https://doi.org/10.1016/j.gca.2021.05.005)

Publication date:
2021

License:
CC BY-ND

Document Version:
Accepted author manuscript

[Link to publication](#)

Citation for published version (APA):
Maeda, R., Goderis, S., Debaille, V., Pourkhorsandi, H., Hublet, G., & Claeys, P. (2021). The effects of Antarctic alteration and sample heterogeneity on Sm-Nd and Lu-Hf systematics in H chondrites. *Geochimica et Cosmochimica Acta*, 305, 106-129. <https://doi.org/10.1016/j.gca.2021.05.005>

Copyright

No part of this publication may be reproduced or transmitted in any form, without the prior written permission of the author(s) or other rights holders to whom publication rights have been transferred, unless permitted by a license attached to the publication (a Creative Commons license or other), or unless exceptions to copyright law apply.

Take down policy

If you believe that this document infringes your copyright or other rights, please contact openaccess@vub.be, with details of the nature of the infringement. We will investigate the claim and if justified, we will take the appropriate steps.

The effects of Antarctic alteration and sample heterogeneity on Sm-Nd and Lu-Hf systematics in H chondrites

Ryoga Maeda^{a,b,*}, Steven Goderis^a, Vinciane Debaille^b, Hamed Pourkhorsandi^b,
Geneviève Hublet^b, Philippe Claeys^a

^a Analytical-, Environmental-, and Geo-Chemistry, Vrije Universiteit Brussel, Pleinlaan 2, BE-1050
Brussels, Belgium.

^b Laboratoire G-Time, Université libre de Bruxelles, CP 160/02, 50, Av. F.D. Roosevelt, BE-1050, Brussels,
Belgium.

* Corresponding author. E-mail address: Ryoga.Maeda@vub.be (R. Maeda)

Abstract

Long-lived radioactive isotope systematics, such as Sm-Nd and Lu-Hf, are useful tools as important chronometers and tracers for chemical differentiation processes. Even though Antarctic meteorites include rare meteorites such as ungrouped, shergottites-nakhlites-chassignites, and lunar meteorites, the effects of Antarctic alteration on the Sm-Nd and Lu-Hf systems in chondrites have not yet been evaluated in detail. Moreover, the heterogeneity of Sm-Nd and Lu-Hf data in bulk chondrites prevents the determinations of precise average Sm-Nd and Lu-Hf values for individual chondrite groups and such robust values of the Chondritic Uniform Reservoir (CHUR). To examine the effects of Antarctic alteration and sample heterogeneity on the Sm-Nd and Lu-Hf isotope systematics, ten Antarctic H chondrites (HCs) and three HCs from hot deserts were characterized for their modal abundances, major and trace elemental concentrations, as well as Sm-Nd and Lu-Hf isotopic compositions. Regardless of the classical weathering index for Antarctic meteorites and the normalized Rb abundance used as a chemical alteration indicator in this study, the modal and elemental abundances in Antarctic HCs appear to be in good agreement with those in non-Antarctic HCs. The Sm-Nd and Lu-Hf isotopic compositions of the characterized H chondrites fall within the range measured for both HC falls and for falls of other chondrite classes, except in the case of the most heavily altered samples. Consequently, the effects of Antarctic alteration processes on the Sm-Nd and Lu-Hf systematics in HCs appear to be limited, except in the case of A 09516 (H6). The latter meteorite exhibits severe mineralogical and chemical alteration, with considerable losses of even the rare earth elements (REEs), which are considered relatively immobile. The $^{147}\text{Sm}/^{144}\text{Nd}$, $^{143}\text{Nd}/^{144}\text{Nd}$, $^{176}\text{Lu}/^{177}\text{Hf}$, and $^{176}\text{Hf}/^{177}\text{Hf}$ of bulk HCs correlate with their P/Mg and Y/Mg. Furthermore, the Lu-Hf ratios are strongly correlated with their P/Ca and Y/Ca as well as their P/Mg and Y/Mg. Thus, the distribution of the elements between constituent minerals in ordinary chondrites (OCs) may control the heterogeneity observed for the bulk Sm-Nd and Lu-Hf data. In this context, the weight ratio of Ca-phosphates to Ca-pyroxene, or at least that of Ca-phosphates to silicates, may be a key factor leading to the observed elemental and isotopic variations. This observation indicates that the nugget effect of Ca-phosphates in OCs as the result of insufficient homogenization or terrestrial alteration leads to the heterogeneities displayed by the Sm-Nd and Lu-Hf data. Moreover, it also indicates that the use

36 of equilibrated OCs for the determination of Sm-Nd and Lu-Hf data is affected more by sample heterogeneity,
37 especially with respect to Ca-phosphates, than is the case for unequilibrated OCs, based on the re-distribution
38 of REEs during thermal metamorphism on their parent bodies. This study demonstrates that Antarctic
39 meteorites commonly preserve their original Sm-Nd and Lu-Hf isotopic compositions as much as chondrite
40 falls, although exceptions are possible in the case of severe alteration. Similar to previous studies, we
41 recommended the use of unequilibrated chondrites, for which the re-distribution of REEs is less extensive,
42 for the determination of well-constrained average Sm-Nd and Lu-Hf isotopic compositions for individual
43 chondrite groups as well as that of the robust Sm-Nd and Lu-Hf CHUR values.

44 1 INTRODUCTION

45 In 1969, a Japanese expedition found nine meteorites in Antarctica, which in 1973 led to the first
46 systematic meteorite recovery expedition on the Southern continent (Yamaguchi *et al.*, 2021), which was
47 followed by expeditions until the present (*e.g.*, Goderis *et al.*, 2021). Today, Antarctic meteorites constitute
48 by number more than half of all known meteorites and include many rare varieties such as ungrouped
49 chondrites and achondrites, shergottites-nakhlites-chassignites, and lunar meteorites (Meteorite Newsletter,
50 NIPR; Antarctic Meteorite Newsletter, NASA). Hence, the Antarctic meteorite collection plays a pivotal role
51 in understanding the history of the Solar System. Meteorites recovered after observed fall events are termed
52 “falls”; those that cannot definitely be associated with observed falls, such as Antarctic meteorites, are named
53 “finds.” Finds are generally characterized by a much longer terrestrial residence time than falls (roughly of
54 the order of tens of kyr: *e.g.*, Al-Kathri *et al.*, 2015). Many finds become weathered during this long residence
55 time, and this process can take place relatively rapidly, particularly in temperate and tropical zones, as well
56 as in hot deserts (Bland *et al.*, 2006; Pourkhorsandi *et al.*, 2021). On average, Antarctic meteorites exhibit
57 old terrestrial ages, on the order of hundreds of kyr (*e.g.*, Nishiizumi *et al.*, 1989), and these are better
58 protected from terrestrial weathering while buried in the ice compared to finds collected from hot deserts
59 (Whillans and Cassidy, 1983; Cassidy and Whillans, 1990). However, these meteorites were exposed to the
60 extreme Antarctic climate during an extended period of time, leading to significant mineralogical and
61 chemical alteration (*e.g.*, Koebel and Cassidy, 1991; Bland *et al.*, 2006).

62 Rare earth elements (REEs) are refractory lithophile elements that share similar chemical properties due
63 to their electron configurations, implying that they should not have been fractionated by condensation and
64 volatilization processes in the early Solar System or by metal-silicate separation during core formation in
65 differentiated planets. Therefore, REEs are universally used for understanding specific planetary processes,
66 such as silicate differentiation. The REEs include long-lived radioactive isotopes such as ^{147}Sm and ^{176}Lu ,
67 which decay to ^{143}Nd (half-life ~ 106 Gyr; Lugmair and Marti, 1978) and ^{176}Hf (half-life ~ 37.1 Gyr; Patchett
68 *et al.*, 2004), respectively. Their isotope systematics form the basis of important chronometers and tracers of
69 chemical differentiation processes. The Sm-Nd and Lu-Hf isotope systematics of chondritic meteorites are
70 particularly important as the Chondritic Uniform Reservoir (CHUR), which constitutes the average reference
71 for undifferentiated planetary material in the Solar System (DePaolo and Wasserburg, 1976). Bouvier *et al.*
72 (2008) determined the currently most precise CHUR values of the Sm-Nd and Lu-Hf data as well as the

73 respective isochrons by utilizing unequilibrated carbonaceous, ordinary, and enstatite chondrites of petrologic
74 types 1-3, mostly from falls, since scatter increases when using equilibrated chondrites. Consequently, the
75 Sm-Nd and Lu-Hf CHUR values are regarded as the equivalents of the composition of Bulk Silicate Earth.
76 As Bouvier *et al.* (2008) discussed, the heterogeneity of Sm-Nd and Lu-Hf data in bulk chondrites is one of
77 the largest problems when willing to determine precise average values (*i.e.*, CHUR values or an average of a
78 group of chondrites), as the observed spread leads to larger uncertainties on the mean. For example, such
79 heterogeneity occurs even on a duplicate analysis of Lu-Hf values in an H4 chondrite ($^{176}\text{Lu}/^{177}\text{Hf} = 0.0301$
80 ± 0.0002 and 0.0334 ± 0.0002 , $^{176}\text{Hf}/^{177}\text{Hf} = 0.282444 \pm 0.000009$ and 0.282761 ± 0.000016 in Ochansk;
81 Patchett *et al.*, 2004).

82 Previous studies regarding Sm-Nd and Lu-Hf systems in bulk chondrites have focused on falls to avoid
83 any possible weathering occurring during long terrestrial residence (*e.g.*, Jacobsen and Wasserburg, 1984;
84 Blichert-Toft and Albarède, 1997, Patchett *et al.*, 2004; Bouvier *et al.*, 2008). Terrestrial weathering can affect
85 REEs, although they are often considered to be relatively immobile (*e.g.*, Shimizu *et al.*, 1983; Crozaz, 2003;
86 Al-Kathri *et al.*, 2015; Pourkhorsandi *et al.*, 2017). The effects of Antarctic alteration on REE abundances
87 were only examined for achondrites, and more specifically for eucrites (Shimizu *et al.*, 1983; Mittlefehldt
88 and Lindstrom, 1991; Crozaz, 2003). Today, few studies exist for chondrites (Tatsumoto *et al.*, 1981;
89 Nishikawa *et al.*, 1990). In particular, the effects of Antarctic alteration on the Sm-Nd and Lu-Hf systems in
90 bulk chondrites remain poorly understood.

91 As such, even though the Antarctic collection includes meteorite groups and clans found only in
92 Antarctica, the effects of Antarctic alteration on Sm-Nd and Lu-Hf systems in chondrites have not been
93 assessed on a systematic way. Therefore, in this study, the results of the Sm-Nd and Lu-Hf isotope systematics
94 in Antarctic HCs are examined in a methodical manner to evaluate weathering effects induced by extended
95 residence times within the Antarctic ice. Moreover, this work also investigates the constituent minerals that
96 control the heterogeneity of these isotope systems in bulk HC by combining the isotopic ratios and elemental
97 abundance ratios, which can aid in determining average Sm-Nd and Lu-Hf isotopic compositions with limited
98 uncertainty (*i.e.*, precise average Sm-Nd and Lu-Hf isotopic compositions) for individual chondrite groups.

99 **2 EXPERIMENTAL**

100 **2.1 Samples**

101 Ten Antarctic HCs and three HCs collected from hot deserts have been characterized for their modal
102 abundances, and elemental and isotope compositions. Four of the Antarctic HCs, Asuka (A) 09436 (H3), A
103 09387 (H4), A 09618 (H5), A 09516 (H6), and the three hot desert HCs, northwest Africa (NWA) 6752 (H3),
104 NWA 6771 (H4), and Sahara 97035 (H5), were provided by the Royal Belgian Institute of Natural Sciences
105 (RBINS), Belgium. Meteorites A-881258 (H3.0), A-880941 (H3.3), Yamato (Y-)793574 (H3.5), Y-790461
106 (H3.7), Allan Hills (ALH) 78084 (H3.9), and Y-790960 (H7) were allocated by the National Institute of Polar
107 Research (NIPR), Japan. Available information on the meteorites is listed in Table 1. To clarify any potential
108 effect of terrestrial weathering on the inner portions of these chondrites - even if the sample visually appears
109 fresh -, only the interior portions were used to avoid as much as possible fusion crust or sample fragments

110 directly affected by terrestrial weathering.

111 **2.2 *In-situ* measurement**

112 Polished thick sections were prepared for all of the meteorites, except in the case of NWA 6752 (H3) when
113 a polished thin section was used. These polished thick and thin sections were analyzed using a Bruker M4
114 Tornado micro-X-ray fluorescence (μ XRF) scanner equipped with a Rh source and two XFlash 430 Silicon
115 Drift detectors at the Vrije Universiteit Brussel (VUB), Belgium. The M4 set up is described in detail in
116 Winter and Claeys (2017), and for each sample, elemental maps of 16 elements (Na, Mg, Al, Si, P, S, Cl, K,
117 Ca, Ti, Cr, Mn, Fe, Ni, and Zn) were obtained. To produce the element maps, the 25 μ m X-ray beam was
118 applied under vacuum conditions (20 mbar), with 10 μ m step size, 1 ms dwell time per point and maximized
119 source energy settings (50 kV, 600 μ A) without a source filter. Constituent minerals in the samples were
120 identified from the elemental maps and their modal abundances were determined using the ImageJ image
121 analysis program, while confirming the nature of these phases using a JEOL JSM-IT300 scanning electron
122 microscope (SEM) equipped with an Oxford energy dispersive spectrometer (EDS) at the SURF research
123 unit of VUB. Uncertainties for the modal abundances determined using this method are estimated to be better
124 than 10% relative.

125 **2.3 Bulk analyses**

126 To examine the effects of sample heterogeneity as well as Antarctic weathering on the Sm-Nd and Lu-Hf
127 systems, a relatively small sample volume was preferred in this study to amplify sample heterogeneity caused
128 by sampling. Approximately 200 mg of fragments of each sample were homogenized using an agate mortar
129 and pestle dedicated to chondrites. No leaching to remove terrestrial materials was applied, even in the case
130 of the three hot desert HCs. Approximately 100 mg of each powdered sample, which is the smallest possible
131 amount to measure the elemental abundances and the isotope compositions based on their detection limits,
132 was dissolved in Teflon beakers using a mixture of ultrapure concentrated HF-HNO₃ (1:3) at 120 °C overnight.
133 Because undigested residue remained in the beakers, possibly including acid-resistant phases such as oxides,
134 the residues were then transferred into Teflon bombs for high-pressure dissolution, using the same acid
135 mixture at 150 °C for 2 days. During the high-pressure dissolution, the supernatants remaining in the first
136 Teflon beaker were evaporated. After the high-pressure dissolution, the solutions in the bombs were added to
137 the Teflon beakers containing the residues of the supernatants. Following evaporation, the residues were
138 dissolved in concentrated HCl and evaporated again. After re-dissolution in 1.5 M HCl with a trace amount
139 of concentrated HF, a ~2% aliquot of each solution was taken for the determination of major and trace
140 elemental abundances. Similarly, a ~5% aliquot of each solution was spiked with mixed ¹⁴⁸Nd-¹⁵⁰Sm and
141 ¹⁷⁶Lu-¹⁷⁹Hf spikes. The spiked aliquots were heated on a hotplate for at least 1 day for spike-sample
142 equilibration.

143 The REEs and Hf were separated from the main fraction by cation exchange chromatography using 2 mL
144 of AG50W-X8 resin (100-200 mesh for the spiked aliquots, 200-400 mesh for the unspiked aliquots). The
145 Hf cut was collected first during the loading of the sample and the following rinsing step using 1.5 M HCl
146 with a trace amount of concentrated HF, while the REE cut was subsequently collected using 6 M HCl. The

147 REE cuts were loaded onto a column with 2 mL of HDEHP resin to separate Nd for both the unspiked and
148 spiked aliquots, and Sm and Lu for the spiked aliquots. The Hf cuts were further purified from Fe by anion
149 exchange chromatography in 6 M HCl using 2 mL of AG1X8 resin (100-200 mesh for the spiked aliquots,
150 200-400 mesh for the unspiked aliquots), and the remaining matrix, especially Ti, was removed on 2 mL of
151 Eichrom LN-Spec resin using 6 M HCl with a trace amount of H₂O₂. Finally, Hf was collected in 4 M HF.
152 The yields of Nd, Sm, Lu, and Hf are estimated to be better than 90%, 95%, 95%, and 90% respectively, for
153 both unspiked and spiked aliquots (Debaille *et al.*, 2007). Total procedural blanks were determined to be \leq
154 26 pg and \leq 10 pg for Nd and Sm, respectively, and \leq 4.5 pg and \leq 20 pg for Lu and Hf, respectively. No
155 blank correction was applied due to these negligible blank levels, even on the spiked aliquots (the blank-to-
156 sample ratios of more than 1%) because they represent insignificant contributions. The chemical procedures
157 outlined here were performed at the Université libre de Bruxelles (ULB), Belgium, and are based on
158 procedures described in detail in Armytage *et al.* (2018) and Debaille *et al.* (2007, 2017). Reference basalt
159 BHVO-2 of the United States Geological Survey was subjected to the same procedures and measured in
160 duplicate to validate the analytical accuracy and reproducibility during the following measurements using
161 inductively coupled plasma-optical emission spectrometry (ICP-OES), quadrupole-ICP-mass spectrometry
162 (Q-ICP-MS), and multiple collector-ICP-MS (MC-ICP-MS). Approximately 50 mg of BHVO-2 was weighed
163 and prepared at similar concentrations for measurement to the chondrite samples for both unspiked and spiked
164 aliquots. Samples A 09436 (H3) and A 09516 (H6) were also analyzed in duplicate. All duplicate analyses
165 were carried out on different powder subsamples.

166 2.3.1 Measurement of major and trace elemental abundances using ICP-OES and Q-ICP-MS

167 The major elemental abundances (Na, Mg, Al, P, K, Ca, Ti, Cr, Mn, Fe, Co, and Ni) were determined
168 using a Thermo Scientific iCAP 7000 Plus Series ICP-OES at ULB. Yttrium was used as the internal standard,
169 and the dilution factors (DFs) for the meteorite samples and the reference basalt were set to be 15,000 and
170 10,000 respectively, using 5% HNO₃.

171 The trace elemental abundances (Cu, Zn, Rb, Sr, Y, Zr, Nb, Ba, REEs, Hf, Th, and U) were determined
172 using an Agilent 7700 ICP-MS at ULB. Measurement solutions were prepared with 5% HNO₃ and all of the
173 measured elements including the high field strength elements were analyzed in 5% HNO₃ without HF. For
174 Q-ICP-MS analysis, In was used as the internal standard, and the DFs for the meteorite samples and the
175 geological reference materials were set to be 2,000 and 6,000, respectively, in order to minimize the influence
176 of non-spectral matrix effects (Ebihara *et al.*, 2020). Although slight analyte loss has been observed during
177 dissolution (Ebihara *et al.*, 2020), no correction for such analyte loss was applied here. Individual single
178 element standards of Ba, Ce, Pr, and Nd were used to correct isobaric interferences from their oxide molecules.
179 The results for the elemental abundances of BHVO-2 ($n = 2$) are shown in Table 2, together with their
180 preferred values (Jochum *et al.*, 2016).

181 2.3.2 Isotope ratio measurement using MC-ICP-MS

182 All of the unspiked and spiked cuts were analyzed in 0.05 M HNO₃ (with 0.05 M HF for the Hf cuts)
183 using the Nu instruments MC-ICP-MS Nu-Plasma II equipped with an Aridus II desolvating nebulizer at

184 ULB. For isotope measurements of Nd, the unspiked Nd cuts were diluted to 20 ppb. The isobaric interference
185 of ^{144}Sm on ^{144}Nd was monitored on mass ^{147}Sm , but no Sm was detected. Measured Nd isotope ratios were
186 normalized to $^{146}\text{Nd}/^{144}\text{Nd} = 0.7219$ using an exponential law following Debaille *et al.* (2007) to correct for
187 instrumental mass fractionation. Measurements of the meteorite samples and BHVO-2 were bracketed by the
188 measurement of a 20 ppb Rennes in-house Nd standard. The measured $^{143}\text{Nd}/^{144}\text{Nd}$ values of the standard
189 were re-calculated to the accepted $^{143}\text{Nd}/^{144}\text{Nd}$ value of the Rennes in-house Nd standard (0.511961; Chauvel
190 and Blichert-Toft, 2001). For isotope measurements of Hf, the unspiked Hf cuts were prepared at 5 ppb.
191 Isobaric interferences for Hf from Yb, Lu, and W were monitored on masses ^{172}Yb , ^{175}Lu , and ^{182}W ,
192 respectively. No detectable Yb, Lu, or W were found in the unspiked Hf cuts. Measured Hf isotope ratios
193 were normalized to $^{179}\text{Hf}/^{177}\text{Hf} = 0.7325$ using the exponential law to correct for instrumental mass
194 fractionation. A 5 ppb JMC-475 Hf standard was used to bracket each sample during the runs. The measured
195 $^{176}\text{Hf}/^{177}\text{Hf}$ values of the Hf standard were re-calculated to the accepted $^{176}\text{Hf}/^{177}\text{Hf}$ value of the JMC-475 Hf
196 standard (0.282163; Blichert-Toft *et al.*, 1997). Internal reproducibilities of Nd and Hf are better than 32 ppm
197 and 31 ppm for all standards, respectively. The means of $^{143}\text{Nd}/^{144}\text{Nd}$ values and $^{176}\text{Hf}/^{177}\text{Hf}$ values in BHVO-
198 2 are 0.512971 ± 0.000012 (2SE, $n = 4$) and 0.283102 ± 0.000011 (2SE, $n = 10$), as shown in Table 2. These
199 values overlap within uncertainty with published reference values (0.512984 ± 0.000011 ; Weis *et al.*, 2006
200 and 0.283105 ± 0.000011 ; Weis *et al.*, 2007, respectively).

201 For spiked cuts, the mass fractionation for each element was corrected using an exponential law followed
202 by spike stripping using an iterative method (Debaille *et al.*, 2007). The same isotopes as in unspiked Nd and
203 Hf analyses were monitored to check for isobaric interferences during spiked Nd and Hf analyses. No
204 detectable contributions of these isotopes were observed in the spiked Nd and Hf cuts. During Sm
205 measurement, ^{147}Sm , ^{150}Sm , ^{152}Sm , and ^{154}Sm were measured. Here, ^{150}Sm is included due to the use of the
206 ^{150}Sm enriched spike despite the isobaric interference by ^{150}Nd . The presence of Nd and Gd in the Sm cuts
207 was monitored on masses ^{146}Nd and ^{156}Gd , and the presence of Gd was corrected mathematically. Even
208 though a trace of Nd was observed in the Sm cuts, the contribution was considered negligible. The isobaric
209 interference of ^{176}Hf was monitored on mass ^{177}Hf during Lu analysis, but no Hf was detected in the Lu cuts.
210 Because Lu possesses only two stable isotopes, a mass fractionation correction for Lu must be applied, for
211 example by using Yb (Blichert-Toft *et al.*, 1997). The uncertainties on the Nd, Sm, Lu, and Hf concentrations
212 are dominated by the uncertainty of the spike calibration, which is estimated to be better than 0.5% (2SE).
213 Therefore, the uncertainties on the concentrations are estimated to be 0.5% as a maximum and are presented
214 in Tables 2 and 4. The obtained $^{147}\text{Sm}/^{144}\text{Nd}$ and $^{176}\text{Lu}/^{177}\text{Hf}$ values for BHVO-2 are 0.1515 ± 0.0011 (2SE)
215 and 0.0088 ± 0.0001 (2SE), shown in Table 2, which are in good agreement with their preferred values of
216 0.1501 ± 0.0010 and 0.00878 ± 0.00006 , respectively (Jochum *et al.*, 2016).

217 **3 RESULTS**

218 **3.1 Modal abundances**

219 Table 3 summarizes the modal abundances in all samples obtained using the μXRF , including the mean
220 values of unequilibrated H chondrites (UHCs; $n = 7$) and equilibrated H chondrites (EHCs; $n = 6$), together

221 with the published modal abundances of EHCs (Van Schmus, 1969; McSween *et al.*, 1991). According to the
222 mineral observation using SEM-EDS in this study, forsterite, silica, and a few accessory minerals (Table 3)
223 can be found in a limited number of samples. Also, H chondrites generally contain ilmenite (~0.2 wt.%: *e.g.*,
224 McSween *et al.*, 1991). However, the mapping using μ XRF is not sufficiently quantitative and the minimum
225 spot size (25 μ m) used in this study is larger than the size of some mineral phases (*e.g.*, silica and ilmenite),
226 which does not allow distinguishing forsterite from low-Ca pyroxene (especially enstatite), silica from
227 feldspar, or ilmenite from chromite. Therefore, the modal abundances of low-Ca pyroxene, feldspar, and
228 chromite obtained in this study include the abundances of forsterite, silica, and ilmenite, respectively.
229 Moreover, grains smaller than ~5 μ m, such as tiny Ca-phosphates especially present in UHCs, might have
230 been missed because of this limitation. However, forsterite and silica are only observed in some UHCs (for
231 forsterite: A-881258, Y-793574, Y-790461, and NWA 6752; for silica: Y-790461 and A 09436) and A 09387
232 (H4), and these were confirmed to be present in the HCs in trace abundances only. Based on this work, there
233 is no resolvable difference in the modal abundances between Antarctic HCs and hot desert HCs, thus the
234 mean values of UHCs and EHCs are calculated from the combined data for Antarctic and hot desert HCs
235 (Fig. 1). Most of the mean modal abundances in UHCs and EHCs are in good agreement with each other
236 (Table 3 and Fig. 1). These mean modal abundances also compare well with the published values listed in
237 Table 3. The mean modal abundance of total Ca-phosphates in EHCs is 0.70 ± 0.10 wt. % at the 95%
238 confidence interval (95% CI) and agrees within uncertainty with previously published values. In addition,
239 the mean modal abundances of chlorapatite and merrillite in UHCs and EHCs overlap within uncertainty
240 (0.10 ± 0.07 wt. % vs. 0.17 ± 0.14 wt. % and 0.29 ± 0.08 wt. % vs. 0.53 ± 0.24 wt. %, respectively at the
241 95% CI; Table 3). However, the mean modal abundance of total Ca-phosphates in UHCs is 0.39 ± 0.09 wt. %
242 (95% CI), which is significantly lower than the abundance in EHCs (Fig. 1).

243 3.2 Elemental abundances

244 The major and trace elemental abundances in bulk samples measured using ICP-OES and ICP-MS are
245 summarized in Table 4, with mean values for the Antarctic UHCs (n = 7), Antarctic EHCs (n = 3), Antarctic
246 HCs (n = 10) and hot desert HCs (n = 3), and literature values for non-Antarctic HCs (Jarosewich, 1990 for
247 Na, Mg, Al, P, K, Ca, Ti, Cr, Mn, Fe, and Ni; Wasson and Kallmeyer, 1988 for Cu, Zn, Rb, Sr, Y, Zr, Nb, Ba,
248 and Hf; Nakamura, 1974 for REEs; Tatsumoto *et al.*, 1973 for Th and U). The data of A 09516 (H6) are
249 excluded from the mean values of Antarctic EHCs and Antarctic HCs because of the anomalous depletions
250 in various elements, including the REEs, displayed by this sample as the result of chemical alteration in
251 Antarctica (*e.g.*, Lipschutz and Samuels, 1991). This sample also exhibits a positive Eu anomaly, as often
252 observed in heavily weathered Antarctic chondrites (*e.g.*, Y-74014: Ebihara, 1986; Y-74492: Nishikawa *et al.*
253 *et al.*, 1990). The characteristics of this sample are described in detail in subsection 4.1.2.

254 3.2.1 Major elements

255 The abundances of major elements for individual samples obtained using ICP-OES were determined with
256 ~2% relative standard deviation (RSD; 1SD) on average, while the individual RSDs ranged from 0.05% to
257 8%. Although most of the mean values for major elemental abundances in Antarctic HCs are in good

258 agreement with the literature values, the mean values of K, Ti, Fe, and Ni are ~15% lower than those reported
259 in literature. However, the mean Ti abundance in Antarctic HCs is in excellent agreement with the published
260 Ti abundance in HCs determined using the isotope dilution method (0.0549 ± 0.0015 wt. % at the 95% CI;
261 calculated from Shima, 1979). According to these results, there is almost no difference in the abundances of
262 major elements between Antarctic and hot desert HCs, although the K and Ca abundances in hot desert HCs
263 are ~20% higher than those in Antarctic HCs possibly due to either mobilization of these elements by
264 chemical alteration in Antarctica (Velbel *et al.* 1991) or terrestrial contamination in hot deserts (Al-Kathiri *et*
265 *al.*, 2005; Pourkhorsandi *et al.*, 2019).

266 3.2.2 Trace elements

267 The trace elemental abundances for individual samples obtained using Q-ICP-MS are reproducible within
268 ~3% RSD (1SD) on average. The abundances of Lu and U in some samples display larger uncertainties, due
269 to their lower absolute abundances, on the order of ~10% RSD. The CI-normalized REE, Th, and U
270 abundances in each sample are shown in Fig. 2, and their mean REE, Th and U abundances in Antarctic
271 UHCs, EHCs, and HCs are compared with the literature values in Fig. 3 (CI values are from Anders and
272 Grevesse, 1989). No resolvable difference is observed between the trace elemental abundances of bulk
273 Antarctic UHCs and EHCs, which is consistent with the conclusions of Huss *et al.* (2006) and Hublet *et al.*
274 (2019). Most of the mean trace elemental abundances in Antarctic HCs, especially for REEs, Th, and U, are
275 in good agreement with the literature values for non-Antarctic HC listed in Table 4. The mean values for Sr
276 and Ba in Antarctic HCs deviate from the literature values (8.82 ± 0.31 ppm vs. 10 ppm and 3.22 ± 0.15 ppm
277 vs. 4.20 ppm at the 95% CI, respectively). However, Sr and Ba are strongly affected by terrestrial weathering
278 as their abundances in the hot desert HCs characterized in this study are high (16.9-70.9 ppm and 17.8-166
279 ppm, respectively). Moreover, the mean values for Sr and Ba in Antarctic HCs are in agreement within
280 uncertainty with their published values for Antarctic HCs determined by the isotope dilution method ($9.29 \pm$
281 0.93 ppm and 2.69 ± 0.75 ppm at the 95% CI; Nishikawa *et al.*, 1990). Thus, the observed deviations may
282 only reflect a difference between Antarctic and non-Antarctic meteorites. For hot desert HCs, the mean values
283 of Cu, Zn, Rb, and Y agree within uncertainty with those for Antarctic HCs in this study and with the literature
284 values for non-Antarctic HC, with the exception of Rb. However, other trace elements are enriched compared
285 with the values of Antarctic HCs and non-Antarctic HCs, especially in the case of Sr, Ba, the light REEs
286 (LREEs), Th, and U. In addition, negative Eu anomalies are observed in the CI-normalized REE patterns of
287 hot desert HCs (Fig. 2).

288 3.3 Isotope compositions

289 The Nd, Sm, Lu, and Hf abundances determined by the isotope dilution method, and Sm-Nd and Lu-Hf
290 isotopic compositions in the bulk samples measured using MC-ICP-MS are summarized in Table 2 (for
291 BHVO-2) and Table 4 (for meteorites) as well as in Figs. 4 and 5. The $^{143}\text{Nd}/^{144}\text{Nd}$ and $^{176}\text{Hf}/^{177}\text{Hf}$ values in
292 most of the samples were determined within 20 ppm relative standard error (RSE) and 60 ppm RSE (2SE),
293 respectively. This relatively large standard error for $^{176}\text{Hf}/^{177}\text{Hf}$ values compared with that for $^{143}\text{Nd}/^{144}\text{Nd}$
294 values clearly results from the difference in the adjusted concentrations in the measurement solutions (see

295 subsection 2.3.2). Furthermore, the actual Hf concentration in the measurement solutions for most of the
296 meteorite samples was less than 5 ppb, leading to larger standard errors for the $^{176}\text{Hf}/^{177}\text{Hf}$ values. On the
297 other hand, the differences in these elemental abundances between those determined using the isotope
298 dilution method (MC-ICP-MS) and calibration line method (Q-ICP-MS) are less than 5% on average, which
299 is in excellent agreement.

300 The mean values of the elemental abundances determined using the isotope dilution method in Antarctic
301 HCs are in excellent agreement with those in HC falls (Table 4). Most of the Sm-Nd and Lu-Hf data for
302 Antarctic HCs are within the range of chondrite fall data and several of them plot on the respective chondrite
303 isochrons within uncertainty (for Sm-Nd data: Jacobsen and Wasserburg, 1980, 1984; Patchett *et al.*, 2004;
304 Boyet and Carlson, 2005; Carlson *et al.*, 2007; Bouvier *et al.*, 2008, Gannoun *et al.*, 2011; Burkhardt *et al.*,
305 2016; Fukai and Yokoyama, 2017; for Lu-Hf data: Blichert-Toft and Albarède, 1997; Bizzarro *et al.*, 2003;
306 Patchett *et al.*, 2004; Bouvier *et al.*, 2008; Dauphas and Pourmand, 2011; for chondrite isochrons: Bouvier
307 *et al.*, 2008). The mean values of $^{147}\text{Sm}/^{144}\text{Nd}$, $^{143}\text{Nd}/^{144}\text{Nd}$, $^{176}\text{Lu}/^{177}\text{Hf}$, and $^{176}\text{Hf}/^{177}\text{Hf}$ for Antarctic HCs
308 overlap with those of HC falls within uncertainties (Table 4). There are no resolvable differences in the mean
309 values of Antarctic UHC and EHC. In the case of hot desert HCs, the $^{147}\text{Sm}/^{144}\text{Nd}$ and $^{143}\text{Nd}/^{144}\text{Nd}$ values
310 (0.1578-0.1866 and 0.512312-0.512540, respectively) are significantly lower than the mean values reported
311 in literature for HC falls (0.1953 ± 0.0006 and 0.512623 ± 0.000009 at 2SE, respectively; Table 4) and the
312 mean values determined here for Antarctic HCs (0.1971 ± 0.0016 and 0.512633 ± 0.000044 at the 95% CI,
313 respectively; Table 4), plotting as far from the isochron as falling out of the range of chondrite fall data (Fig.
314 4). In contrast, it seems that the $^{176}\text{Lu}/^{177}\text{Hf}$ and $^{176}\text{Hf}/^{177}\text{Hf}$ values of hot desert HCs fall within the ranges
315 determined in literature and measured for Antarctic HCs (Table 4 and Fig. 5), except in the case of NWA
316 6771 (H4), which is characterized by an anomalously high Hf abundance (269 ppb).

317 **4 DISCUSSION**

318 **4.1 Assessment of weathering effects on the Sm-Nd and Lu-Hf systems in Antarctic HCs**

319 For the assessment of weathering effects on Antarctic meteorites, the classical ABC index system is
320 commonly used: A—minor rustiness (*e.g.*, rust stains along fractures are minor); B—moderate rustiness (*e.g.*,
321 7.5 to 35% of metal particles are weathered to limonite); C—severe rustiness (*e.g.*, most metal particles are
322 weathered to limonite); and e—evaporite minerals are visible to the naked eye (Antarctic Meteorite
323 Newsletter, NASA; Meteorite Newsletter, NIPR). However, this index may not be sufficient as an indicator
324 especially in terms of chemical alteration (Koebel and Cassidy, 1991), as it is determined based on mineralogy.
325 Velbel (1988) and Nishikawa *et al.* (1990) found that bulk Rb abundances in some Antarctic ordinary
326 chondrites (OCs) and heavily weathered non-Antarctic HCs are anomalously low and do not co-vary with
327 the weathering index. Velbel (1988) concluded that Rb loss could be due to chemical leaching during the
328 residence of the meteorite in Antarctica, indicating that relative loss of Rb may be a better indicator of
329 chemical alteration than the weathering index. The results presented here display remarkable deviations in
330 the Rb abundances of both Antarctic and hot desert HCs relative to those reported in literature (Table 4). The
331 mean Rb abundance of Antarctic HCs is significantly lower than the literature value (2.26 ± 0.34 ppm vs. 2.9

332 ppm at the 95% CI) with extremely low Rb abundances in A-880941 (H3.3) and A 09516 (H6), implying a
333 loss of Rb during Antarctic alteration. However, these lower Rb abundances may just reflect heterogeneity
334 in the amount of feldspar in the samples, which may be induced as the result of a sampling bias (*i.e.*, sampling
335 heterogeneity), as Rb is mostly distributed in feldspar (Shima and Honda, 1968; Mason and Graham, 1970).
336 The average Na and Al abundances in the bulk samples are used as an indicator for the amount of feldspar in
337 the sample, and the respective Rb abundances normalized to the indicator are listed in Table 5. Even
338 considering the heterogeneous distribution of feldspar based on these normalized Rb abundances, the samples
339 displaying extremely low Rb abundances also show low normalized Rb abundances. Thus, any possible effect
340 on the bulk Rb abundance by sampling biases alone can be ruled out. The normalized Rb abundances can
341 also be compared with the normalized abundances of Sr, which is especially concentrated in feldspar (Shima
342 and Honda, 1968; Mason and Graham, 1970) but generally considered less mobile than Rb. The data from
343 this study are compared with calculated values for non-Antarctic HC (Table 4) and Antarctic HCs from
344 Nishikawa *et al.* (1990), in Fig. 6. The normalized Sr abundances in most of the samples are in good
345 agreement with the literature values, but in various samples the normalized Rb abundances are lower than
346 those reported in literature and display a wider range than the Sr abundances. A similar trend emerges when
347 comparing the normalized abundance of Rb and that of Ba, which is concentrated in feldspar as well (Table
348 5). The low normalized Rb abundances (< 2.7) in some Antarctic HCs co-vary to some degree with their
349 weathering grades, although exceptions exist. A-880941 (H3.3) is categorized as A/B but contains a low
350 normalized Rb abundance (1.77 ± 0.09), which may reflect a difference in the weathering degree implied by
351 elemental ratios versus that inferred based on petrographic observation. In any case, the low Rb abundances
352 clearly reflect the loss of Rb during the terrestrial residence of the meteorites in Antarctica or elsewhere in
353 the world (Nishikawa *et al.*, 1990), possibly because of chemical leaching. Therefore, the normalized Rb
354 abundances are taken here as a potential indicator for chemical alteration in the following discussions.

355 4.1.1 Weathering effects on bulk Sm-Nd and Lu-Hf systems

356 The Sm-Nd and Lu-Hf data of a few Antarctic HCs (*e.g.*, A 09516) plot away from the respective chondrite
357 isochrons (Figs. 4 and 5). This may reflect an effect of weathering on the Sm-Nd and Lu-Hf systems in bulk
358 chondrites in Antarctica. However, it remains unclear whether the parent isotopic ratios $^{147}\text{Sm}/^{144}\text{Nd}$ and
359 $^{176}\text{Lu}/^{177}\text{Hf}$ or the daughter isotopic ratios $^{143}\text{Nd}/^{144}\text{Nd}$ and $^{176}\text{Hf}/^{177}\text{Hf}$ have been affected by Antarctic
360 weathering. Alternatively, it is also possible that both ratios were disturbed. Therefore, we need to consider
361 one by one which of the following processes affected the Sm-Nd and Lu-Hf systems: i) sample heterogeneity,
362 ii) thermal metamorphism on the parent body(ies), iii) contamination with terrestrial material, and iv)
363 chemical alteration during residence on the Earth.

364 i) Based on the results of this study and previous works, REEs in bulk chondrites are largely
365 unfractionated (*e.g.*, Huss *et al.*, 2006). On the other hand, REEs in individual constituent minerals are highly
366 fractionated depending on their partition coefficients (*e.g.*, Curtis and Schmitt, 1979). This fractionation of
367 REEs between the constituent minerals affects not only their abundances but also their radiogenic isotope
368 systems (*e.g.*, Jacobsen and Wasserburg, 1983). Thus, a loss of constituent mineral(s) due to terrestrial
369 weathering, as observed in Antarctic eucrites (Mittlefehldt and Lindstrom, 1991), or a non-representative

370 sampling bias may induce minor variation in the elemental compositions and radiogenic isotope data of bulk
371 chondrites. According to Amelin and Rotenberg (2004), Amelin (2005), and Debaille *et al.* (2017), the Sm-
372 Nd and Lu-Hf data in individual minerals are indeed different from those in bulk chondrites. However, both
373 data of individual minerals and bulk chondrites plot on the same chondrite isochron when considering the
374 uncertainties. Therefore, the heterogeneous distribution of constituent mineral(s) due to a sampling bias or
375 terrestrial weathering, *i.e.*, sample heterogeneity may result in heterogeneity of the Sm-Nd and Lu-Hf data of
376 bulk chondrites, but the isotopic data will always plot along the isochrons.

377 ii) Thermal metamorphism can affect the Sm-Nd and Lu-Hf systems at the bulk scale as a redistribution
378 due to crystallization of REE-rich minerals such as Ca-phosphates, can take place during metamorphism
379 (Bouvier *et al.*, 2008; Martin *et al.*, 2013; Debaille *et al.*, 2017; Bloch *et al.*, 2017, 2018). The nugget effect,
380 in which the REE-rich Ca-phosphates are heterogeneously distributed, can lead to sampling biases due to
381 non-representative sample volumes, while such Ca-phosphate phases may also be preferentially weathered
382 during the terrestrial residence of the meteorite of interest. These processes may produce wider ranges in the
383 Sm-Nd and Lu-Hf data in bulk equilibrated chondrites than in bulk unequilibrated chondrites (Bouvier *et al.*,
384 2008; Dauphas and Pourmand, 2011, 2015). However, as mentioned above, unequilibrated and equilibrated
385 chondrites do not show any fractionation or change in the bulk REE abundances in most of the cases. If
386 unequilibrated and equilibrated chondrites had originally the exact same bulk elemental composition, the
387 bulk Sm-Nd and Lu-Hf data in these chondrites should exhibit the same values. This is consistent with the
388 observation that the mean Sm-Nd and Lu-Hf values in bulk unequilibrated and equilibrated chondrites are in
389 agreement with each other, both based on this study and literature values (Jacobsen and Wasserburg, 1980,
390 1984; Blichert-Toft and Albarède, 1997; Bizzarro *et al.*, 2003; Patchett *et al.*, 2004; Boyet and Carlson, 2005;
391 Carlson *et al.*, 2007; Bouvier *et al.*, 2008, Dauphas and Pourmand, 2011; Gannoun *et al.*, 2011; Burkhardt *et al.*,
392 2016; Fukai and Yokoyama, 2017). Therefore, thermal metamorphism emphasizes the heterogeneity of
393 the Sm-Nd and Lu-Hf data in bulk chondrites at the scale of the individual sample. Theoretically, the isotopic
394 data in bulk unequilibrated and equilibrated chondrites should have the same values as long as these have the
395 same elemental compositions.

396 iii) Considering the higher Nd, Sm, Lu, and Hf abundances and lower $^{147}\text{Sm}/^{144}\text{Nd}$ and $^{176}\text{Lu}/^{177}\text{Hf}$ in the
397 upper continental crust (26 ppm, 4.5 ppm, 0.32 ppm, 5.8 ppm, 0.10, and 0.0079, respectively; Taylor and
398 McLennan, 1995) as potential contaminating material relative to the lower REE concentrations in chondrites,
399 the Sm-Nd and Lu-Hf data in bulk chondrites display lower values in most of the cases when terrestrial
400 contamination occurred (Bast *et al.*, 2017a, b; Pourkhorsandi *et al.*, 2017, 2021). As the hot desert HCs used
401 in this study exhibit enrichments in Sr, Ba, LREEs, Th, and U and negative Eu anomalies (Table 4 and Fig.
402 2), these enrichments must result from terrestrial contamination (*e.g.*, Al-Kathiri *et al.*, 2005; Pourkhorsandi
403 *et al.*, 2017). Thus, the low $^{147}\text{Sm}/^{144}\text{Nd}$ and $^{143}\text{Nd}/^{144}\text{Nd}$ values in the hot desert HCs (Table 4 and Fig. 4)
404 must also be explained by mixing with terrestrial material. However, the absolute Lu abundance in the upper
405 continental crust is only ~10 times higher than that in HCs and Hf is highly immobile during terrestrial
406 alteration, while the absolute abundances of Nd and Sm in the upper continental crust are ~45 and ~25 times
407 higher than those in HCs, respectively (Taylor and McLennan, 1995), and these elements are also considered
408 to be more mobile than Hf (Middelburg *et al.*, 1988). In this way, because it is more difficult for the Lu-Hf

409 system to be affected by terrestrial contamination than the Sm-Nd system, the $^{176}\text{Lu}/^{177}\text{Hf}$ and $^{176}\text{Hf}/^{177}\text{Hf}$
410 values in the hot desert HCs used in this study do not deviate as far from the isochron as observed for the
411 $^{147}\text{Sm}/^{144}\text{Nd}$, $^{143}\text{Nd}/^{144}\text{Nd}$ values (Table 4 and Fig. 5). This is consistent with the observation of Al-Kathiri *et*
412 *al.* (2005) who showed that Hf abundances in HCs collected from hot deserts do not deviate from the literature
413 value listed in Table 4 (0.15-0.18 ppm vs. 0.18 ppm), while their corresponding Nd and Sm abundances are
414 ~10-30% higher than the literature values (0.66-0.75 ppm vs. 0.59 ppm and 0.21-0.24 ppm vs. 0.19 ppm,
415 respectively). Therefore, although the extent of terrestrial contamination on chondrites strongly depends on
416 where the sample was collected (Pourkhorsandi *et al.*, 2017, 2021), this process can produce deviations from
417 the Sm-Nd and Lu-Hf isochrons in the case of chondrites (Bast *et al.*, 2017b). These deviations should be
418 accompanied by additional indications of terrestrial contamination, such as higher abundances of Sr, Ba,
419 LREEs, Th, and U.

420 iv) Chemical alteration during terrestrial residence, such as leaching, occurs anywhere on Earth in the
421 presence of water, either in the form of rain or humidity. Even in Antarctica, melting of ice can trigger sample
422 alteration (Mittlefehldt and Lindstrom, 1991). Chemical alteration is commonly divided into two main types:
423 the first type encompasses alteration affecting minerals, such as the loss of Ca-phosphates (Mittlefehldt and
424 Lindstrom, 1991), while the second type reflects alteration that depends on the mobility of the element, as in
425 the case of Rb loss (Velbel, 1988; Nishikawa *et al.*, 1990). For the former type of alteration, the effect on the
426 Sm-Nd and Lu-Hf systems is similar to the effect of sample heterogeneity. Thus, even if this alteration occurs,
427 the affected Sm-Nd and Lu-Hf data would plot on their respective isochrons assuming no prior disturbance.
428 The latter type of alteration can disturb these systems because the parent nuclide and the daughter nuclide
429 may have different chemical characteristics, which is consistent with the observations of Nishikawa *et al.*
430 (1990) although based on the Rb-Sr system. Thus, if this alteration occurred during the residence of the
431 meteorite at the Earth's surface, the $^{147}\text{Sm}/^{144}\text{Nd}$ and $^{176}\text{Lu}/^{177}\text{Hf}$ values would be disturbed producing
432 deviations from the Sm-Nd and Lu-Hf isochrons. This type of alteration does not influence the $^{143}\text{Nd}/^{144}\text{Nd}$
433 and $^{176}\text{Hf}/^{177}\text{Hf}$ values at the bulk scale.

434 In summary, thermal metamorphism amplifies the nugget effect of REE-rich minerals such as Ca-
435 phosphates on the Sm-Nd and Lu-Hf isotope systems. Sample heterogeneity also affects the Sm-Nd and Lu-
436 Hf data in bulk chondrites, but the measured data continue to plot on the respective chondrite isochrons. In
437 addition, $^{143}\text{Nd}/^{144}\text{Nd}$ and $^{176}\text{Hf}/^{177}\text{Hf}$ values are not affected by chemical alteration at the bulk scale or at
438 least such isotopic fractionation is not yet resolvable. Thus, the $^{143}\text{Nd}/^{144}\text{Nd}$ and $^{176}\text{Hf}/^{177}\text{Hf}$ values obtained
439 likely reflect the original values of the bulk HC sample, unless this sample was contaminated by terrestrial
440 material. Because the Asuka, Yamato, and Allan Hill samples used in this study are collected from blue ice
441 fields, it is unlikely that the samples were contaminated during their residence in Antarctica. Therefore, the
442 deviations from the isochrons on the Sm-Nd and Lu-Hf data that are apparent in a small set of samples (Figs.
443 4 and 5) have likely been produced by disturbance of the $^{147}\text{Sm}/^{144}\text{Nd}$ and $^{176}\text{Lu}/^{177}\text{Hf}$ values during the
444 chemical alteration that depends on the elemental mobility.

445 Based on the assumption above, to evaluate the effects of Antarctic weathering on the Sm-Nd and Lu-Hf
446 data in bulk chondrites, the differences in $^{147}\text{Sm}/^{144}\text{Nd}$ and $^{176}\text{Lu}/^{177}\text{Hf}$ values between the measured values
447 and the respective chondrite isochrons are expressed as $\delta^{147}\text{Sm}/^{144}\text{Nd}$ (‰) and $\delta^{176}\text{Lu}/^{177}\text{Hf}$ (‰) respectively,

448 calculated following the equations (in the case of the Sm-Nd system):

$$449 \quad \delta \frac{^{147}\text{Sm}}{^{144}\text{Nd}} = \left[\left(\frac{^{147}\text{Sm}}{^{144}\text{Nd}} \right)_{\text{measured}} - \left(\frac{^{147}\text{Sm}}{^{144}\text{Nd}} \right)_{\text{ideal}} \right] \times 1,000 \text{ [‰]}$$

450 and

$$451 \quad \left(\frac{^{147}\text{Sm}}{^{144}\text{Nd}} \right)_{\text{ideal}} = \frac{\left(\frac{^{143}\text{Nd}}{^{144}\text{Nd}} \right)_{\text{measured}} - b}{a}$$

452 where a is the slope of the isochron and b is the intercept of the isochron, which is the initial $^{143}\text{Nd}/^{144}\text{Nd}$
453 value. The values for the isochrons and the initial isotope ratios in Sm-Nd and Lu-Hf systems are from
454 Bouvier *et al.* (2008). These calculated differences for Antarctic HCs reflect the extent of the disturbance on
455 the $^{147}\text{Sm}/^{144}\text{Nd}$ and $^{176}\text{Lu}/^{177}\text{Hf}$ values by Antarctic alteration. The calculated differences are shown in Fig.
456 7, with a range of differences in chondrite falls since the Sm-Nd and Lu-Hf data in chondrite falls also show
457 a deviation from the isochron (Figs. 4 and 5). According to Fig. 7, the $\delta^{147}\text{Sm}/^{144}\text{Nd}$ values of Antarctic HCs,
458 except for A 09436 (H3)-2, ALH 78084 (H3.9), and A 09516 (H6), fall within the range of HC falls taking
459 into account the associated uncertainty. The $\delta^{176}\text{Lu}/^{177}\text{Hf}$ of Antarctic HCs, except for Y-793574 (H3.5), Y-
460 790461 (H3.7), A 09387 (H4), and A 09618 (H5), also fall within the range of HC falls. Although the
461 $\delta^{147}\text{Sm}/^{144}\text{Nd}$ or $\delta^{176}\text{Lu}/^{177}\text{Hf}$ values of the samples excluded above do not fall within the range of HC falls,
462 the $\delta^{147}\text{Sm}/^{144}\text{Nd}$ and $\delta^{176}\text{Lu}/^{177}\text{Hf}$ values of all Antarctic HCs, except for A 09516 (H6)-1, do plot within the
463 range of other chondrite falls. The values of Antarctic HCs that do not fall within the range of HC falls could
464 indicate disturbance of the systems by chemical alteration in Antarctica. However, this disturbance can be
465 considered minor as most of the values fall within the range of other chondrite falls. The $\delta^{147}\text{Sm}/^{144}\text{Nd}$ and
466 $\delta^{176}\text{Lu}/^{177}\text{Hf}$ values in A-880941 (H3.3), which displays the lowest weathering index but the second highest
467 Rb loss in this study, fall close to 0. Similar $\delta^{147}\text{Sm}/^{144}\text{Nd}$ and $\delta^{176}\text{Lu}/^{177}\text{Hf}$ values are observed for heavily
468 weathered (sub)samples A 09618 (H5) and A 09436 (H3)-2 respectively, and for A-881258 (H3.0) that
469 indicates no Rb loss. Furthermore, $\delta^{147}\text{Sm}/^{144}\text{Nd}$ and $\delta^{176}\text{Lu}/^{177}\text{Hf}$ values of all published data for Antarctic
470 chondrites (Figs. 4 and 5), except for ALHA 77295 (EH3) with a high $\delta^{147}\text{Sm}/^{144}\text{Nd}$ (5.66‰), range from -
471 1.96 to 1.94‰ and from -0.02 to 0.18‰, respectively, falling within the range of chondrite falls also
472 regardless of their weathering index. Therefore, it can be concluded that Antarctic chondrites display limited
473 effects of weathering on their isotopic values, and the extent of the disturbance on $^{147}\text{Sm}/^{144}\text{Nd}$ and
474 $^{176}\text{Lu}/^{177}\text{Hf}$ in Antarctic chondrites would be of a level similar to that measured for chondrite falls even if
475 Antarctic weathering occurred. In addition, there seems to be no correlation between the $\delta^{147}\text{Sm}/^{144}\text{Nd}$ and
476 $\delta^{176}\text{Lu}/^{177}\text{Hf}$ values and the weathering indicators, suggesting that both the Sm-Nd and Lu-Hf systems are
477 fairly robust against Antarctic weathering relative to the Rb-Sr system (Nishikawa *et al.*, 1990). However,
478 the most weathered sample in this study, as indicated by the weathering index C and the lowest normalized
479 Rb abundance (Table 5), A 09516 (H6), shows the largest absolute $\delta^{147}\text{Sm}/^{144}\text{Nd}$ values in this study and an
480 atypical CI-normalized REE signature that is characterized by subchondritic values and a positive Eu
481 anomaly (Figs. 2 and 7). Therefore, the Sm-Nd and Lu-Hf systems are generally unaffected by Antarctic
482 weathering except in the case of anomalous CI-normalized REE abundances, as all samples except A 09516
483 (H6) display normal chondritic REE patterns and low $\delta^{147}\text{Sm}/^{144}\text{Nd}$ and $\delta^{176}\text{Lu}/^{177}\text{Hf}$ values.

485 As described above, A 09516 clearly underwent a significant degree of alteration, both mineralogically
486 and chemically. Since this sample was analyzed in duplicate and the low elemental abundances are observed
487 for this sample twice, significant sample losses during acid decomposition can be ruled out. Moreover, no
488 other sample analyzed in this study exhibits such low abundances. Given that the weathering mechanism that
489 affected A 09516 appears considerably more complicated than that of any other sample, this H6 chondrite is
490 excluded from the previous discussions and is discussed here separately.

491 The low P and REE abundances and the P/Mg of A 09516 relative to the other HCs (Tables 4 and 5) may
492 imply a loss of Ca-phosphates, known to take place during the alteration of eucrites in Antarctica (Mittlefehldt
493 and Lindstrom, 1991). However, the characteristic LREE depletion and Ce anomaly typical for alteration of
494 Antarctic eucrites are not observed A 09516 (Fig. 2). Considering the CI-normalized REE abundance in Ca-
495 phosphates of HCs (Ebihara and Honda, 1983; Ward *et al.*, 2017), HCs that have lost Ca-phosphates should
496 display lower CI-normalized LREE abundances relative to the heavy REE (HREE) abundances, which
497 indicates that the CI-normalized REE abundances in A 09516 cannot be explained only by a loss of Ca-
498 phosphates, as is the case for the weathered Antarctic eucrites (Mittlefehldt and Lindstrom, 1991). Normal
499 chondritic Th and U abundances in A 09516 (Table 4 and Fig. 2) support that this sample did not lose
500 considerable Ca-phosphate, simply because Th and U are also concentrated in Ca-phosphates of OCs (Pellas
501 and Störzer, 1975; Crozaz, 1979). Generally, OCs, including HCs, contain chlorapatite and merrillite as Ca-
502 phosphates (*e.g.*, Van Schmus, 1969). The CI-normalized REE abundances in merrillite are relatively flat,
503 while those in chlorapatite are more enriched in LREEs than in HREEs in OCs (Crozaz *et al.*, 1989; Ward *et al.*,
504 2017). In addition, the Th and U abundances in merrillite are considerably lower (~ 3 ppm and ~ 0.3 ppm,
505 respectively) than those in chlorapatite (~ 11 ppm and ~ 7.5 ppm, respectively) for OCs (Crozaz, 1974, 1979),
506 implying that a loss of merrillite from bulk OCs affects the bulk Th and U abundances significantly less than
507 a loss of chlorapatite. Thus, the REE abundances in A 09516 might be explained by the selective or more
508 rapid dissolution of merrillite rather than chlorapatite during Antarctic alteration. However, the solubilities
509 of merrillite and chlorapatite are comparable under acidic conditions (Adcock *et al.*, 2013), and selective or
510 rapid dissolution of merrillite is hence unlikely. Therefore, a simple loss of Ca-phosphates by alteration
511 cannot explain the elemental composition of A 09516.

512 Alternatively, chemical leaching depending on the solubility of an element, for example taking place at
513 grain boundaries, could explain the elemental losses observed for A 09516. It is assumed that this mechanism
514 does not strongly affect the mineralogy of the OCs, as highly mobile elements are leached more during this
515 type of alteration. According to studies dealing with the mobility of REEs during weathering (Nesbitt, 1979;
516 Middelburg *et al.*, 1988; van der Weijden and van der Weijden, 1995; Hannigan and Sholkovitz, 2001; Su *et al.*,
517 2017), the middle REEs (MREEs) and HREEs can more strongly be leached than the LREEs by alteration
518 depending on the redox conditions, which could produce the observed REE abundances in A 09516. This can
519 leave immobile elements such as Hf and Th in this sample. Moreover, the solubility difference explains the
520 large deviation from the isochron on the Sm-Nd plots for A 09516 (Figs. 4 and 7) because any weathering
521 mechanism affecting the modal abundance of the constituent minerals, such as a loss of Ca-phosphates, could

522 not induce this divergence. However, the positive Eu anomaly in A 09516 cannot be produced by this leaching
523 mechanism because the sample would exhibit no or rather a negative Eu anomaly if leaching occurred
524 following their solubilities only. In addition, the Lu/Hf data in A 09516 display only a limited deviation
525 ($\delta\text{Lu/Hf} = -1.32 \pm 0.23 \text{ ‰}$; Figs. 5 and 7) from the isochron while the Sm-Nd data show a larger deviation
526 ($\delta\text{Sm/Nd} = -5.58 \pm 1.40 \text{ ‰}$ and $-10.5 \pm 1.4 \text{ ‰}$; Figs. 4 and 7), which is inconsistent with their relative mobility.
527 Therefore, the chemical leaching depending on the solubility of an element can also not fully explain the
528 characteristics of A 09516.

529 Lastly, two speculative possibilities remain to explain the REE abundances in A 09516: either some Ca-
530 phosphates were partially leached during Antarctic alteration, or some Ca-phosphates were completely
531 leached during Antarctic alteration, but the sample was at a later stage contaminated by terrestrial material.
532 Similar scenarios have been proposed by Bast *et al.* (2017b) to explain the observed discrepancies from the
533 reference isochron for bulk Lu-Hf data in eucrites and angrites. In the case of the former scenario, Ca-
534 phosphates are fractured to some extent by an interruption in the ionic bonding between cations, especially
535 impurity cations, and $(\text{PO}_4)^{2-}$ in the Ca-phosphates as the result of Antarctic alteration, but the Ca-phosphates
536 are not completely broken due to insufficiencies in time, in the amount of fluid, or in the pH of the fluid
537 during the leaching. This leads to selective leaching of more soluble trace elements from Ca-phosphates. In
538 this case, the losses of MREEs and HREEs are more remarkable than those of LREEs, while the positive Eu
539 anomaly and the normal Th and U abundances in A 09516 remain. Moreover, this incomplete dissolution of
540 Ca-phosphates can produce the disturbance on the Sm-Nd plots for A 09516. However, the observation of a
541 lack of disturbance for the Lu/Hf in A 09516 still remains to be explained. In the case of the latter scenario,
542 contamination by terrestrial material during residence in Antarctica (Delisle *et al.*, 1989; Welten *et al.*, 2001)
543 or during the experimental procedure such as sample crushing cannot be ruled out completely, although the
544 contamination during Antarctic residence is unlikely because other samples, collected in the vicinity of A
545 09516, show no traces of contamination based on the results in this study. In both cases of contamination,
546 some Ca-phosphates are removed by leaching during Antarctic alteration entirely, but the abundances of
547 LREEs, Th, and U in A 09516 remain elevated because of terrestrial contamination. This can also explain the
548 disturbance of Sm/Nd, the presence of the positive Eu anomaly and even the absence of any disturbance of
549 the Lu/Hf because of less pronounced effects from terrestrial contamination on the Lu and Hf abundances.
550 However, the observation that the Th and U abundances are still chondritic limits the possible admixture of
551 terrestrial material. In any case, both possibilities including the loss of Ca-phosphates are inconsistent with a
552 high modal abundance of Ca-phosphates in this sample (0.75 wt. %; Table 3), although their mass scales need
553 to be considered. Therefore, A 09516 may have lost some amount of Ca-phosphates, but the way this HC lost
554 Ca-phosphates appears to be different from how Antarctic eucrites are affected (Mittlefehldt and Lindstrom,
555 1991), indicating that Antarctic alteration may be significantly more complicated than what is expected based
556 on heavily altered samples.

557 **4.2 Control of heterogeneity on bulk Sm-Nd and Lu-Hf data by Ca-phosphates and Ca-pyroxene**

558 The isotopic heterogeneity mostly depends on the sample heterogeneity unless the sample is affected by
559 terrestrial weathering, as discussed above. Thus, it is important to constrain which minerals mainly affect the

560 Sm-Nd and Lu-Hf data of bulk chondrites. To do this, elemental abundance ratios in Antarctic HCs were
561 compared with their isotope ratios, and their correlation coefficients r are shown in Table 6. If a constituent
562 mineral controls the heterogeneity in bulk Sm-Nd and Lu-Hf data, elements accommodated in the mineral
563 should display co-variation with the isotope data, if no selective removal or addition of elements occurred
564 during weathering. According to the correlation coefficients for all samples, P/Mg and Y/Mg display strong
565 positive correlations with $^{147}\text{Sm}/^{144}\text{Nd}$, $^{176}\text{Lu}/^{177}\text{Hf}$, and $^{176}\text{Hf}/^{177}\text{Hf}$ ($r = 0.5-0.8$) and strong negative
566 correlations with $^{143}\text{Nd}/^{144}\text{Nd}$ ($r = -0.6$ and -0.7 , respectively). If A 09516 (H6) is excluded, because its
567 $^{147}\text{Sm}/^{144}\text{Nd}$ is the most disturbed by Antarctic weathering among the samples studied in this work, the P/Mg
568 displays a strong negative correlation with $^{147}\text{Sm}/^{144}\text{Nd}$ instead of a positive correlation ($r = -0.6$; Table 6).
569 In the case of OCS, Y is distributed in Ca-phosphates (*e.g.*, Mason, 1970), and Ca-phosphates have lower
570 $^{147}\text{Sm}/^{144}\text{Nd}$ and $^{143}\text{Nd}/^{144}\text{Nd}$ values and higher $^{176}\text{Lu}/^{177}\text{Hf}$ and $^{176}\text{Hf}/^{177}\text{Hf}$ values compared to bulk samples
571 (Amelin and Rotenberg, 2004; Amelin, 2005; Debaille *et al.*, 2017). Thus, these correlations indicate that the
572 isotope ratios in bulk samples highly depend on the Ca-phosphates-to-silicates weight ratio in the sample,
573 because the P/Mg and Y/Mg can be considered as indicators of the Ca-phosphates/silicates.

574 The correlation coefficients excluding A 09516 (H6) are shown in Table 6, not only because of the reasons
575 outlined above but also because this sample is characterized by an abnormally low abundance of Ca-
576 phosphates as discussed in the subsection 4.1.2. When A 09516 (H6) is excluded, the P/Mg no longer
577 correlates with the $^{176}\text{Lu}/^{177}\text{Hf}$ and $^{176}\text{Hf}/^{177}\text{Hf}$. Because the Y/Mg still correlates with these ratios and P is in
578 part distributed in metals especially in unequilibrated chondrites (Murrell and Burnett, 1983; Zanda *et al.*,
579 1994), this may be caused by a disturbance of the bulk P abundance through the accommodation of P in metal.
580 On the other hand, Al/Mg, Ca/Mg, and Ti/Mg display negative correlations with $^{176}\text{Lu}/^{177}\text{Hf}$ and $^{176}\text{Hf}/^{177}\text{Hf}$
581 ($r = -0.8$ to -0.4), although the correlations with Al/Mg are relatively weak ($r = -0.4$ and -0.5 , respectively).
582 According to *in-situ* analyses and Hf partition coefficients of minerals (Alexander, 1994; Righter and Shearer,
583 2003; Martin *et al.*, 2013), Hf is distributed in chondrule glass and Ca-pyroxene in unequilibrated chondrites
584 and in Ca-pyroxene in equilibrated chondrites. Aluminum, Ca, and Ti are distributed in these silicate minerals
585 as well, although Al is mostly distributed in feldspar in EOCs (Curtis and Schmitt, 1979; Alexander, 1994).
586 Considering the REE distribution in EOCs, Lu is not only distributed in Ca-phosphates but also partitioned
587 to a large degree into Ca-pyroxene, while Sm and Nd are mostly distributed in Ca-phosphates (*e.g.*, Curtis
588 and Schmitt, 1979). In the case of UOCs, Lu is distributed in chondrule glass and Ca-pyroxene (Alexander,
589 1994; Shinotsuka, 1997). In addition, chondrule glass has the lowest Lu/Hf among silicates and Ca-
590 phosphates for unequilibrated chondrites and Ca-pyroxene has the lowest Lu/Hf among these minerals for
591 equilibrated chondrites (Alexander, 1994; Martin *et al.*, 2013). Therefore, the negative correlations of Al/Mg,
592 Ca/Mg, and Ti/Mg with $^{176}\text{Lu}/^{177}\text{Hf}$ and $^{176}\text{Hf}/^{177}\text{Hf}$ indicate that the amount of Ca-pyroxene, which is a major
593 host phase of Hf and a partial carrier of Lu, affects the heterogeneity of bulk Lu-Hf data. Moreover, the
594 negative correlations are also produced by the heterogeneity in the amount of chondrule glass, which is a
595 major host phase of Lu and Hf in UHCs. The negative correlation between Ti/Mg and Lu-Hf data may also
596 be affected by the amount of ilmenite, which can have lower Lu/Hf than that in Ca-pyroxene according to
597 their partition coefficients (Green, 1994; Kleine *et al.*, 2008). However, considering the budget of Hf between
598 constituent minerals in the whole rock, the correlation mostly depends on the weight ratio of Ca-pyroxene to

599 silicates (or Ca-pyroxene and chondrule glass to silicates).

600 According to Table 6, P/Ca and Y/Ca exhibit negative correlations with Sm-Nd and positive
601 correlations with Lu-Hf data, both when including and excluding A 09516 (H6), although $^{147}\text{Sm}/^{144}\text{Nd}$ still
602 displays positive correlations possibly because of the disturbance by weathering. Most of these correlations
603 are stronger than those for the P/Mg and Y/Mg. For OCs, REEs including Y are mostly distributed among
604 the two phases of Ca-phosphate and Ca-pyroxene (Ehigara and Honda, 1984). Among silicates and Ca-
605 phosphates in chondrites, Ca-phosphates have the highest P/Ca, Y/Ca, and Lu/Hf and the lowest Sm/Nd (*e.g.*,
606 Curtis and Schmitt, 1979; Amelin, 2005). In contrast, Ca-pyroxene has the lowest P/Ca, Lu/Hf, and Y/Ca and
607 the highest or second highest Sm/Nd (Curtis and Schmitt, 1979; Alexander, 1994; Martin *et al.*, 2013). Thus,
608 Ca-phosphates and Ca-pyroxene are considered to be the endmembers of the bulk P/Ca, Y/Ca, Sm/Nd, and
609 Lu/Hf, indicating that the correlations of the P/Ca and Y/Ca reflect the Ca-phosphates-to-Ca-pyroxene weight
610 ratio. Therefore, the heterogeneity of Sm-Nd and Lu-Hf data in bulk OCs is mainly controlled by the weight
611 ratio of Ca-phosphates to Ca-pyroxene in the sample. For UOCs, the amount of chondrule glass also affects
612 the overall REE budget and isotopic values.

613 **4.3 Relationship between the distributions of REEs and Hf and the heterogeneities of bulk Sm-Nd and** 614 **Lu-Hf data**

615 According to the result of the *in-situ* measurement in this study, the modal abundance of Ca-phosphates
616 in UHCs is significantly lower than that in EHCs (Fig. 1). This increase in the modal abundances of Ca-
617 phosphates from UHCs to EHCs must result from thermal metamorphism on their parent body(ies) (Huss *et*
618 *al.*, 2006). On the other hand, the bulk REE and P abundances overlap within uncertainty between UHCs and
619 EHCs, which is consistent with previous works (*e.g.*, Jarosewich, 1990). Murrell and Burnett (1983) reported
620 that Ca-phosphate grains in UOCs are very fine ($< 10 \mu\text{m}$). Perron *et al.* (1992) found phosphate, chromite,
621 silica, and silica inclusions as secondary minerals in some UOCs. However, Semarkona (LL3.00), which is
622 one of the least metamorphosed chondrites, does not contain such grains. Based on these observations,
623 combining the bulk P abundances and the modal abundances of Ca-phosphates between UHCs and EHCs
624 used in this study, Ca-phosphates must have formed and grown in a closed system during thermal
625 metamorphism on the parent body or bodies. Ehigara (1989) and Shinotsuka (1997) analyzed REE
626 abundances in acid residues of OCs with lower and higher degrees of metamorphism, which were leached
627 using HCl or HNO₃. Because REEs are enriched in chondrule glass in UOCs (Alexander, 1994), Shinotsuka
628 (1997) suggested that the REEs are re-distributed mainly from chondrule glass to Ca-phosphates during
629 thermal metamorphism. Since the bulk REE abundances are the same between UOCs and EOCs, the re-
630 distribution of REEs may have occurred in a closed system with the growth of Ca-phosphates. This REE re-
631 distribution in a closed system can explain the observation that the Sm-Nd and Lu-Hf data of each constituent
632 mineral in chondrites are plotted on the respective chondrite isochrons (Amelin and Rotenberg, 2004; Amelin,
633 2005; Debaille *et al.*, 2017). In this way, because REEs are more distributed to Ca-phosphates in EOCs than
634 UOCs, the nugget effect of Ca-phosphates for EOCs produces larger isotopic variabilities of Sm-Nd and Lu-
635 Hf systematics than that for UOCs, which reinforces the conclusions by Bouvier *et al.* (2008) and Dauphas
636 and Pourmand (2011, 2015). Moreover, sampling effects on bulk Lu-Hf data due to a heterogeneous

637 distribution of Ca-pyroxene may be larger in EOCs than in UOCs because Lu is hosted in Ca-pyroxene as
638 well as Ca-phosphates, while Hf seems to be re-distributed from chondrule glass to Ca-pyroxene based on
639 their initial distribution and their re-distribution after metamorphism (Curtis and Schmitt, 1979; Alexander,
640 1994; Righter and Shearer, 2003; Martin *et al.*, 2013), although no data exist on the Hf distribution in OCs
641 and the mobility of Hf during thermal metamorphism. These larger contributions to bulk Sm-Nd and Lu-Hf
642 data by the sampling heterogeneities of Ca-phosphates and Ca-pyroxene in EOCs in terms of the distributions
643 of REE and Hf are complementary to the correlations between the elemental abundance ratios and the isotopic
644 ratios obtained in this study (Table 6). Therefore, unequilibrated chondrites in which the re-distributions have
645 not proceeded in the case of OCs should be used for the determination of precise average Sm-Nd and Lu-Hf
646 isotopic compositions to limit the effects of the sampling heterogeneities, reinforcing the conclusions by
647 Bouvier *et al.* (2008) and Debaille *et al.* (2017). Even in this case, the sampling heterogeneity of chondrule
648 glass can still lead to heterogeneity in the bulk Sm-Nd and Lu-Hf data although the effect on the isotope data
649 by the heterogeneous distribution of chondrule glass appears to be less than that by the heterogeneous
650 distribution of Ca-phosphates. Theoretically, equilibrated chondrites could also be useful for the
651 determination of precise average isotopic compositions as aimed for the CHUR values if a sufficiently large
652 amount of the sample is homogenized (speculatively more than a few grams at least), because the
653 heterogeneity of bulk Sm-Nd and Lu-Hf data only results from the sample heterogeneity, provided that re-
654 distributions occurred in a closed system. Based on Patchett *et al.* (2004) and Bouvier *et al.* (2008), the mean
655 values and uncertainties of bulk Sm-Nd data in equilibrated chondrites are almost the same as those in
656 unequilibrated chondrites when a few grams of equilibrated chondrite are homogenized ($^{147}\text{Sm}/^{144}\text{Nd} =$
657 0.1960 ± 0.0006 and 0.1960 ± 0.0004 ; $^{143}\text{Nd}/^{144}\text{Nd} = 0.512634 \pm 0.000012$ and 0.512630 ± 0.000011 ,
658 respectively) On the other hand, the homogenization with even a few grams of equilibrated chondrite seems
659 to be insufficient for the determination of bulk average Lu-Hf isotopic compositions for the purpose of CHUR
660 determination ($^{176}\text{Lu}/^{177}\text{Hf} = 0.0324 \pm 0.0009$ and 0.0336 ± 0.0001 ; $^{176}\text{Hf}/^{177}\text{Hf} = 0.282693 \pm 0.000078$ and
661 0.282785 ± 0.000011 , the same order as above), as also concluded by Patchett *et al.* (2004). Thus, equilibrated
662 chondrites may provide representative Sm-Nd isotopic compositions in individual samples as long as more
663 than a few grams of the sample is homogenized to remove the nugget effect, and such data would be useful
664 for the determination of precise average Sm-Nd isotopic compositions for individual chondrite groups.
665 However, because of the uncertainty related to the essential mass to be actually representative, only
666 unequilibrated chondrites should be used for the determination of the precise Lu-Hf CHUR values, probably
667 applied to the determination of precise average Sm-Nd isotopic compositions for individual chondrite groups
668 as well. This difference in sufficient sample amounts for homogenization may be because the variation in
669 Sm-Nd data largely depends on the sampling heterogeneity of Ca-phosphates, while the variation in Lu-Hf
670 data depends not only on the sampling heterogeneity of Ca-phosphates but also on that of Ca-pyroxene and
671 chondrule glass.

672 The distributions of REEs and Hf and the redistribution of these elements during parent body processes
673 differ between the various classes of chondrites as the major hosts of those elements and their parent body
674 processes vary, as shown in Table 7, although the distribution and the mobility of Hf remain poorly
675 understood. Sampling biases involving these major hosts are largely responsible for the observed variations

676 in Sm-Nd and Lu-Hf isotopic ratios. For example, CV and CO chondrites contain abundant Ca, Al-rich
677 inclusions (CAIs; 2.98 vol.% and 0.99 vol.%, respectively; Hezel *et al.*, 2008), producing variable REE
678 abundances and probably variable Hf abundance as well, as the result of a heterogeneous distribution of CAIs
679 in samples of these meteorites. However, CI-normalized abundances of REEs in bulk CAIs are only $\sim 20 \times \text{CI}$
680 (*e.g.*, El Goresy *et al.*, 2002), while bulk oldhamite in enstatite chondrites and bulk Ca-phosphates in R
681 chondrites contain $\sim 100 \times \text{CI}$ and $\sim 200 \times \text{CI}$ of REEs, respectively (Laimmer and Ganapathy, 1987; Maeda *et al.*,
682 2017a). Moreover, other refractory components such as amoeboid olivine aggregates contain much less REE
683 and Hf abundances (Krot *et al.*, 2004). Thus, based on mass balance considerations, the nugget effects of
684 CAIs or other refractory components on the Sm-Nd and Lu-Hf isotopic heterogeneities are not as much as
685 those of Ca-phosphates or oldhamite. In the cases of enstatite and Rumuruti chondrites, the modal abundances
686 of the REE host phases are only less than 2 wt. % and about 0.4 wt. %, respectively (Crozzaz and Lundberg,
687 1995; Bischoff *et al.*, 2011). Moreover, Barrat *et al.* (2014) and Maeda *et al.* (2017b) concluded that the REEs
688 of both chondrite types were re-distributed between the respective host phases during thermal metamorphism.
689 Thus, similar to OCs, the unequilibrated counterparts of these other chondrite classes should be preferred to
690 determine the precise average Sm-Nd and Lu-Hf isotopic compositions for enstatite and Rumuruti chondrites
691 to avoid strong nugget effects of the respective host phases. This may also apply to CK chondrites because
692 these experienced thermal metamorphism and contain < 1 vol. % of Ca-phosphates as one of the hosts of
693 REEs (Martin *et al.*, 2013). Kakangari, CV, and CO chondrites underwent aqueous alteration but
694 simultaneously also underwent a limited degree of thermal metamorphism on their parent bodies. However,
695 their thermal metamorphism occurred within the unequilibrated range, implying the effect of elemental re-
696 distribution by thermal metamorphism is almost negligible. For many groups of carbonaceous chondrites that
697 underwent aqueous alteration, it is unclear whether heavily altered samples can be used for the determination
698 of the precise average isotopic compositions because the redistribution of REEs and Hf during aqueous
699 alteration remains poorly constrained. According to Bouvier *et al.* (2008), aqueously altered samples produce
700 fewer heterogeneities of bulk Sm-Nd and Lu-Hf data than metamorphosed samples. Therefore, the use of
701 unequilibrated chondrites not only for OCs but also for most other classes of chondrites can reduce the effect
702 of variability in the isotope data stemming from the sample heterogeneity, which is required for the
703 determination of precise average Sm-Nd and Lu-Hf isotopic compositions for individual chondrite groups.

704 **5 CONCLUSIONS**

705 In this study, we analyzed ten Antarctic HCs and three HCs from hot deserts in a systematic manner to
706 determine their modal mineral abundances, major and trace elemental abundances, and Sm-Nd and Lu-Hf
707 isotopic compositions. The following conclusions can be drawn.

708 Firstly, by calculating the Rb abundances normalized to the average Na and Al abundances for each
709 sample to evaluate Antarctic chemical alteration, our results indicate that not all weathered samples
710 categorized as C according to the weathering index display a loss of Rb. Conversely, samples categorized as
711 A/B may exhibit a high Rb loss. Thus, the normalized Rb abundance can be a good indicator for the
712 assessment of Antarctic alteration chemically but only indicates the relative intensity of the chemical

713 weathering in Antarctica.

714 Secondly, the effects of Antarctic alteration on the Sm-Nd and Lu-Hf systems in bulk HCs are evaluated
715 using the $\delta^{147}\text{Sm}/^{143}\text{Nd}$ and $\delta^{176}\text{Lu}/^{177}\text{Hf}$ notations. These values do not correlate with the weathering index
716 or the Rb indicator, except in the case of a single heavily weathered sample A 09516 (H6), which displays
717 various element losses, including for the REEs. This result suggests that the Sm-Nd and Lu-Hf systems
718 preserve their original compositions during Antarctic alteration. However, when a sample is heavily affected
719 by Antarctic weathering and has lost many elements, the isotope systems may also be disturbed. Such high
720 elemental losses might reflect partial dissolution of Ca-phosphates during alteration. Therefore, unless the
721 sample is clearly heavily weathered, most Antarctic meteorites, including rare meteorites such as ungrouped,
722 shergottites-nakhlites-chassignites, and lunar meteorites can be used for the investigation of their Sm-Nd and
723 Lu-Hf isotopic compositions.

724 Finally, we confirm that the Sm-Nd and Lu-Hf data in bulk HCs are correlated with the weight ratio of
725 Ca-phosphates to silicates. The weight ratio of Ca-phosphates to Ca-pyroxene may correlate stronger with
726 the isotopic ratios, especially in the case of the Lu-Hf system. Sample heterogeneity of Ca-phosphates in HCs
727 may thus lead to heterogeneities in the bulk Sm-Nd and Lu-Hf data. Since REEs in OCs are re-distributed to
728 Ca-phosphates in a closed system during thermal metamorphism on the parent body(ies), the nugget effect
729 of Ca-phosphates on the heterogeneities of bulk Sm-Nd and Lu-Hf isotope data is larger for EOCs than for
730 UOCs. Therefore, the use of UOCs should be preferred for the determination of well-constrained average
731 Sm-Nd and Lu-Hf isotopic compositions such as CHUR values unless at least a few grams of EOCs are used,
732 which reinforces the conclusion by Bouvier *et al.* (2008). The preferred use of unequilibrated specimens may
733 also be extended to the other classes of chondrites, but the optimal sample amount for homogenization to
734 obtain representative Sm-Nd and Lu-Hf isotopic compositions in a sample is expected to differ for each class
735 because the host phases of REEs and Hf and their remobilization during parent body processes are distinct.
736 For the analysis of bulk isotope data, major and trace elemental abundances should be determined together
737 with the isotope data in order to evaluate the sample heterogeneity and to assess the effects of weathering. A
738 better understanding of the Hf distribution on the bulk meteorite scale, the Hf mobilization during thermal
739 metamorphism, and the redistribution of REEs and Hf during aqueous alteration on meteorite parent bodies
740 may help to determine the sample sizes required to overcome sample heterogeneity and to measure
741 representative Sm-Nd and Lu-Hf isotopic compositions in individual samples, leading to precise average Sm-
742 Nd and Lu-Hf isotopic compositions for individual chondrite groups.

743 **Acknowledgments**

744 We would like to thank S. Cauchies and W. Deboige for assistance in the lab, J. De Jong for helping with
745 the isotope analysis, and N. J. de Winter for guidance with the μXRF . We also thank the Royal Belgian
746 Institute of Natural Sciences, Belgium, and the National Institute of Polar Research, Japan, for the loan of
747 the Antarctic meteorites and meteorites collected from hot deserts used in this study. RM, SG, VD and PhC
748 acknowledge support from the Excellence of Science (EoS) project "ET-HoME". SG, VD and GH thank the
749 BRAIN-Be Belgian Science Policy (BELSPO) project "BAMM". VD thanks the ERC StG ISoSyC and FRS-

750 FNRS for support. HP acknowledges receiving funding from the European Union's Horizon 2020 research
751 and innovation program under the Marie Skłodowska-Curie grant agreement No 801505. PhC acknowledges
752 support from the VUB Strategic Research Program and the Research Foundation Flanders (FWO Hercules
753 grant) for the purchase of the μ XRF instrument. Finally, we are grateful to Audrey Bouvier for her editorial
754 work and insightful comments during the review process. We also thank Erik Scherer, Minako Righter, and
755 an anonymous reviewer for their constructive and detailed reviews.

756 REFERENCES

- 757 Adcock C. T., Hausrath E. M. and Forster P. M. (2013) Readily available phosphate from minerals in early
758 aqueous environments on Mars. *Nat. Geosci.* **6**, 824-827.
- 759 Alexander C. M. O'D. (1994) Trace element distributions within ordinary chondrite chondrules: Implications
760 for chondrule formation conditions and precursors. *Geochim. Cosmochim. Acta* **58**, 3451-3468.
- 761 Al-Kathiri A., Hofmann B. A., Jull J. T. and Gnos E. (2005) Weathering of meteorites from Oman: Correlation
762 of chemical and mineralogical weathering proxies with ^{14}C terrestrial ages and the influence of soil chemistry.
763 *Meteorit. Planet. Sci.* **40**, 1215-1239.
- 764 Amelin Y. (2005) Meteorite phosphates show constant ^{176}Lu decay rate since 4557 million years ago. *Science*
765 **310**, 839-841.
- 766 Amelin Y. and Rotenberg E. (2004) Sm–Nd systematics of chondrites. *Earth Planet. Sci. Lett.* **223**, 267-282.
- 767 Anders E. and Grevesse N. (1989) Abundances of the elements: Meteoritic and solar. *Geochim. Cosmochim.*
768 *Acta* **53**, 197-214.
- 769 Armytage R. M. G., Debaille V., Brandon A. D. and Agee C. B. (2018) A complex history of silicate
770 differentiation of Mars from Nd and Hf isotopes in crustal breccia NWA 7034. *Earth and Planet. Sci. Lett.*
771 **502**, 274-283.
- 772 Barosch J., Ebel D.S., Hezel D. C., Alpert S. and Palme H. (2020) Formation of chondrules and matrix in
773 Kakangari chondrites. *Earth and Planet. Sci. Lett.* **542**, 116286.
- 774 Barrat J. A., Zanda B., Jambon A. and Bollinger C. (2014) The lithophile trace elements in enstatite chondrites.
775 *Geochim. Cosmochim. Acta* **128**, 71-94.
- 776 Bast R., Scherer E. E. and Bischoff A. (2017a) The ^{176}Lu - ^{176}Hf systematics of ALM-A: A sample of the recent
777 Almahata Sitta meteorite fall. *Geochem. Pers. Lett.* **3**, 45–54.
- 778 Bast R., Scherer E. E., Sprung P., Mezger K., Fischer-Gödde M., Taetz S., Böhnke M., Schmid-Beurmann
779 H., Münker C., Kleine T. and Srinivasan G. (2017b). Reconciliation of the excess ^{176}Hf conundrum in
780 meteorites: Recent disturbances of the Lu-Hf and Sm-Nd isotope systematics. *Geochim. Cosmochim. Acta*
781 **212**, 303–323.

782 Bischoff A., Vogel N. and Roszjar J. (2011) The Rumuruti chondrite group. *Chemie der Erde* **71**, 101-133.

783 Bizzarro M., Baker J. A., Haack H., Ulfbeck D. and Rosing, M. (2003) Early history of the Earth's crust–
784 mantle system inferred from hafnium isotopes in chondrites. *Nature* **421**, 931-933.

785 Bland P. A., Zolensky M. E., Benedix G. K. and Sephton M. A. (2006) Weathering of chondritic meteorites.
786 In *Meteorites and the Early Solar System II* (eds. Lauretta D. S. and McSween Jr. H. Y.). The University of
787 Arizona Press, Tucson, pp. 853-867. in collaboration with Lunar and Planetary Institute, Houston.

788 Blichert-Toft J. and Albarède F. (1997) The Lu–Hf isotope geochemistry of chondrites and the evolution of
789 the mantle–crust system. *Earth Planet. Sci. Lett.* **148**, 243-258.

790 Blichert-Toft J., Chauvel C. and Albarède F. (1997) Hf and Lu for high-precision isotope analysis of rock
791 samples by magnetic sector-multiple collector ICP-MS. *Contrib. Mineral. Petrol.* **127**, 248-260.

792 Bloch E., Watkins J. and Ganguly J. (2017) Diffusion kinetics of lutetium in diopside and the effect of thermal
793 metamorphism on Lu–Hf systematics in clinopyroxene. *Geochim. Cosmochim. Acta* **204**, 32-51.

794 Bloch E., Watkins J. and Ganguly J. (2018) Comment on “Reconciliation of the excess ^{176}Hf conundrum in
795 meteorites: Recent disturbances of the Lu-Hf and Sm-Nd isotope systematics” [Geochim. Cosmochim. Acta
796 212 (2017) 303–323]. *Geochim. Cosmochim. Acta* **230**, 190-192.

797 Bouvier A., Vervoort J. D. and Patchett P. J. (2008) The Lu–Hf and Sm–Nd isotopic composition of CHUR:
798 Constraints from unequilibrated chondrites and implications for the bulk composition of terrestrial planets.
799 *Earth Planet. Sci. Lett.* **273**, 48-57.

800 Burkhardt C., Borg L. E., Brennecke G. A., Shollenberger Q. R., Dauphas N. and Kleine T. (2016) A
801 nucleosynthetic origin for the Earth’s anomalous ^{142}Nd composition. *Nature* **537**, 394-398.

802 Boyet M. and Carlson R. W. (2005) Chondrite barium, neodymium, and samarium isotopic heterogeneity
803 and early Earth differentiation. *Science* **316**, 1175-1178.

804 Carlson R. W., Boyet M. and Horan M. (2007) ^{142}Nd evidence for early (>4.53 Ga) global differentiation of
805 the silicate. *Science* **309**, 576-581.

806 Chauvel C. and Blichert-Toft J. (2001) A hafnium isotope and trace element perspective on melting of the
807 depleted mantle. *Earth Planet. Sci. Lett.* **190**, 137-151.

808 Crozaz G. (1974) U, Th and extinct ^{244}Pu in the phosphates of the St. Severin meteorite. *Earth Planet. Sci.*
809 *Lett.* **23**, 164-169.

810 Crozaz G. (1979) Uranium and thorium microdistributions in stony meteorites. *Geochim. Cosmochim. Acta*
811 **43**, 127-136.

812 Crozaz G. and Lundberg L. L. (1995) The origin of oldhamite in unequilibrated enstatite chondrites. *Geochim.*
813 *Cosmochim. Acta* **59**, 3817-3831.

814 Crozaz G., Pellas P., Bourot-Denise M., de Chazal S. M., Fieni C., Lundberg L. L. and Zinner E. (1979)
815 Plutonium, uranium and rare earths in the phosphates of ordinary chondrites—The quest for a chronometer.
816 *Earth Planet. Sci. Lett.* **93**, 157-169.

817 Crozaz G., Floss C. and Wadhwa M. (2003) Chemical alteration and REE mobilization in meteorites from
818 hot and cold deserts. *Geochim. Cosmochim. Acta* **67**, 4727-4741.

819 Curtis D. B. and Schmitt R. A. (1979) The petrogenesis of L-6 chondrites: insights from the chemistry of
820 minerals. *Geochim. Cosmochim. Acta* **43**, 1091-1103.

821 Dauphas N. and Pourmand A. (2011) Hf–W–Th evidence for rapid growth of Mars and its status as a
822 planetary embryo. *Nature* **473**, 489.

823 Dauphas N. and Pourmand A. (2015) Thulium anomalies and rare earth element patterns in meteorites and
824 Earth: Nebular fractionation and the nugget effect. *Geochim. Cosmochim. Acta* **163**, 234-261.

825 Davis A. M. (2006) Volatile evolution and loss. In *Meteorites and the Early Solar System II* (eds. Lauretta D.
826 S. and McSween Jr. H. Y.). The University of Arizona Press, Tucson, pp. 295–307. in collaboration with
827 Lunar and Planetary Institute, Houston.

828 Debaille V., Brandon A. D. Yin Q. Z. and Jacobsen B. (2007) Coupled ^{142}Nd – ^{143}Nd evidence for a protracted
829 magma ocean in Mars. *Nature* **450**, 525-528.

830 Debaille V., Orman J. V., Yin Q. Z. and Amelin Y. (2017) The role of phosphates for the Lu–Hf chronology
831 of meteorites. *Earth Planet. Sci. Lett.* **473**, 52-61.

832 Delisle G., Schultz L., Spettel B., Weber H. W., Wlotzka F., Hofle H. C., Thierbach R., Vogt S., Herpers U.,
833 Bonani G. and Suter M. (1989) Meteorite finds near the Frontier Mountain Range in North Victoria Land.
834 *Geol. Jb.* **38**, 483-513.

835 DePaolo D. J. and Wasserburg G. J. (1976) Nd isotopic variations and petrogenetic models. *Geophys. Res.*
836 *Lett.* **3**, 249–252.

837 Ebihara M. (1987) Determination of ten lanthanoids in chondritic meteorites by radiochemical neutron
838 activation analysis using coaxial and planar type pure Ge detectors. *J. Radioanal. Nucl. Chem.* **111**, 385-397.

839 Ebihara M. (1988) Trace element composition and distribution of Yamato-691, an unequilibrated enstatite
840 chondrite. *Proc. NIPR Symp. Antract. Meteorites* **1**, 102-112.

841 Ebihara M. (1989) Rare earth and some other elements in acid-residues of unequilibrated ordinary chondrites.
842 *Proc. NIPR Symp. Antract. Meteorites* **2**, 279-287.

843 Ebihara M., Hayano K. and Shirai N. (2020) Determination of trace rare earth elements in rock samples
844 including meteorites by ICP-MS coupled with isotope dilution and comparison methods. *Anal. Chim. Acta*
845 **1101**, 81-89.

846 Ebihara M. and Honda M. (1983) Rare earth abundances in chondritic phosphates and their implications for
847 early stage chronologies. *Earth and Planet. Sci. Lett.* **63**, 433-445.

848 Ebihara M. and Honda M. (1984) Distribution of rare earth elements and uranium in various components of
849 ordinary chondrites. *Meteoritics* **19**, 69-77.

850 Ebihara M. and Honda M. (1987) Rare earth elements in Ca-phosphates of Allende carbonaceous chondrite.
851 *Meteoritics* **3**, 179-190.

852 El Goresy A., Zinner E., Matsunami S., Palme H., Spettel B., Lin Y. and Nazarov M. (2002) Efremovka
853 101.1: A CAI with ultrarefractory REE patterns and enormous enrichments of Sc, Zr, and Y in Fassaite and
854 Perovskite. *Geochim. Cosmochim. Acta* **66**, 1459-1491.

855 Fukai R. and Yokoyama T. (2017) Neodymium isotope heterogeneity of ordinary and carbonaceous
856 chondrites and the origin of non-chondritic ^{142}Nd compositions in the Earth. *Earth Planet. Sci. Lett.* **474**, 206-
857 214.

858 Gannoun A., Boyet M., Rizo H. and El Goresy A. (2011) ^{146}Sm - ^{142}Nd systematics measured in enstatite
859 chondrites reveals a heterogeneous distribution of ^{142}Nd in the solar nebula. *Proc. Natl. Acad. Sci.* **108**, 7693-
860 7697.

861 Goderis S., Yesiltas M., Pourkhorsandi H., Shirai N., Poudelet M., Martin L., Yamaguchi A., Debaille V. and
862 Claeys Ph. (2021) Detailed record of the BELARE 2019-2020 meteorite recovery expedition on the Nansen
863 Ice Field, East Antarctica. *Antarctic Record* **65**, 1-20.

864 Green T. H. (1994) Experimental studies of trace-element partitioning applicable to igneous petrogenesis —
865 Sedona 16 years later. *Chem. Geol.* **117**, 1-36.

866 Hannigan R. E. and Sholkovitz E. R. (2001) The development of middle rare earth element enrichments in
867 freshwaters: Weathering of phosphate minerals. *Chem. Geol.* **175**, 495-508.

868 Hezel D. C., Russell S. S., Ross A. J. and Kearsley A. T. (2008) Modal abundances of CAIs: Implications
869 for bulk chondrite element abundances and fractionations. *Meteorit. Planet. Sci.* **43**, 1879-1894

870 Hublet G., Yamaguchi A., Debaille V., Shirai N. and Kimura M. (2019) Geochemical study of type 3 ordinary
871 chondrites. In *the 82nd Ann. Mtg. Met. Soc.*, #6257. LPI Contribution No. 2157, Lunar and Planetary Institute,
872 Houston (abstract).

873 Huss G. R., Rubin A. E. and Grossman J. N. (2006) Thermal metamorphism in chondrites. In *Meteorites and*
874 *the Early Solar System II* (eds. Lauretta D. S. and McSween Jr. H. Y.). The University of Arizona Press,
875 Tucson, pp. 567–586. in collaboration with Lunar and Planetary Institute, Houston.

876 Jacobsen S. B. and Wasserburg G. J. (1980) Sm–Nd isotopic evolution of chondrites. *Earth Planet. Sci. Lett.*
877 **50**, 139-155.

878 Jacobsen S. B. and Wasserburg G. J. (1984) Sm–Nd isotopic evolution of chondrites and achondrites, II.
879 *Earth Planet. Sci. Lett.* **67**, 137-150.

880 Jarosewich E. (1990) Chemical analyses of meteorites: A compilation of stony and iron meteorite analyses.
881 *Meteoritics* **25**, 323-337.

882 Jochum M. P., Weis U., Scwager B., Stoll B., Wilson S. A., Haug G. H., Andreae M. O. and Enzweiler J.
883 (2016) Reference values following ISO guidelines for frequently requested rock reference materials.
884 *Geostand. Geoanal. Res.* **40**, 333-350.

885 Kleine T., Touboul M., Van Orman J. A., Bourdon B., Maden C., Mezger K. and Halliday A. (2008) Hf–W
886 thermochronometry: closure temperature and constraints on the accretion and cooling history of the H
887 chondrite parent body. *Earth Planet. Sci. Lett.* **270**, 106–118

888 Koebel C. and Cassidy W. (1991) Differences between Antarctic and non-Antarctic meteorites: An
889 assessment. *Geochim. Cosmochim. Acta* **55**, 3-18.

890 Krot A. N., Keil K., Scott E. R. D., Goodrich C. A. and Weisberg M. K. (2003) Classification of meteorites.
891 In *Meteorites, Comets, and Planets*, Treatise on Geochemistry (ed. Davis A. M.). Elsevier, Amsterdam, vol.
892 1, chap. 1.05, pp. 83-128.

893 Krot A. N., Petaev M. I., Russell S. S., Itoh S., Fagan T. J., Yurimoto H., Chizmadia L., Weisberg M. K.,
894 Komatsu M., Ulyanov A. A. and Keil K. (2004) Amoeboid olivine aggregates and related objects in
895 carbonaceous chondrites: records of nebular and asteroid processes. *Chemie der Erde* **64**, 185-239.

896 Larimer J. W. and Ganapathy R. (1987) The trace element chemistry of CaS in enstatite chondrites and some
897 implications regarding its origin. *Earth and Planet. Sci. Lett.* **84**, 123-134.

898 Lugmair G. W. and Marti K. (1978) Lunar initial $^{143}\text{Nd}/^{144}\text{Nd}$: differential evolution of the lunar crust and
899 mantle. *Earth Planet Sci. Lett.* **39**, 349-357.

900 Maeda R., Shirai N. and Ebihara M. (2017a) Distribution of rare earth elements, Th and U in R chondrite. In
901 *Lunar Plant. Sci.* **XLVIII**, #2370. Lunar and Planetary Institute, Houston (abstract).

902 Maeda R., Shirai N., Yamaguchi A. and Ebihara M. (2017b) Formation process and metamorphism on R
903 chondrite parent body based on distribution of rare earth elements, Th and U. In *The Eighth Symposium on*
904 *Polar Science*, #00258. National Institute of Polar Science, Tokyo (abstract).

905 Martin C., Debaille V., Lanari P., Goderis S., Vandendael I., Vanhaecke F., Vidal O. and Claeys Ph. (2013)
906 REE and Hf distribution among mineral phases in the CV–CK clan: A way to explain present-day Hf isotopic
907 variations in chondrites. *Geochim. Cosmochim. Acta* **120**, 496-513.

908 Mason B. and Graham A.L. (1970) Minor and trace elements in meteoritic minerals. *Smithson. Contrib. Earth*
909 *Sci.* **3**, 1-17.

- 910 McSween Jr. H. Y., Bennett III M. E. and Jarosewich E. (1991) The mineralogy of ordinary chondrites and
911 implications for asteroid spectroscopy. *Icarus* **90**, 107-116.
- 912 Middelburg J. J., van der Weijden C. H. and Woittiez J. R. W. (1988) Chemical processes affecting the
913 mobility of major, minor and trace elements during weathering of granitic rocks. *Chem. Geol.* **68**, 253-273.
- 914 Mittlefehldt D. W. and Lindstrom M. M. (1991) Generation of abnormal trace element abundances in
915 Antarctic eucrites by weathering processes. *Geochim. Cosmochim. Acta* **55**, 77-87.
- 916 Murrell M. T. and Burnett D. S. (1983) The behavior of actinides, phosphorus, and rare earth elements during
917 chondrite metamorphism. *Geochim. Cosmochim. Acta* **47**, 1999-2014.
- 918 Nakamura N. (1974) Determination of REE, Ba, Fe, Mg, Na and K in carbonaceous and ordinary chondrites.
919 *Geochim. Cosmochim. Acta* **38**, 757-775.
- 920 Nesbitt H. W. (1979) Mobility and fractionation of rare earth elements during weathering of a granodiorite.
921 *Nature* **279**, 206-210.
- 922 Nishiizumi K., Elmore D. and Kubik P. W. (1989) Update on terrestrial ages of Antarctic meteorites. *Earth*
923 *Planet. Sci. Lett.* **93**, 299-313.
- 924 Nishikawa Y., Nakamura N., Misawa K., Okano O., Kagami H. and Yamamoto K. (1990) Investigation of
925 the Weathering Effect on Rb-Sr Systematics and Trace Element Abundances in Antarctic and Non-Antarctic
926 Meteorites: A Case of H-Chondrites. *Mass Spectrosc.* **38**, 115-123.
- 927 Patchett P. J., Vervoort J. D., Soderlund U. and Salters V. J. M. (2004) Lu–Hf and Sm–Nd isotopic systematics
928 in chondrites and their constraints on the Lu–Hf properties of the Earth. *Earth Planet. Sci. Lett.* **222**, 29-41.
- 929 Pellas P. and Störzer D. (1975) Uranium and plutonium in chondritic phosphates. *Meteoritics* **10**, 471
930 (abstract).
- 931 Perron C., Zanda B., Bourot-Denise M., and Mostefaoui S. (1992) Bishunpur and Semarkona: New clues to
932 the origin of inclusions in metal. *Meteoritics* **27**, 275-276.
- 933 Pourkhorsandi H., D'Orazio M., Rochette P., Valenzuela M., Gattacceca J., Mirnejad H., Sutter B., Hutzler
934 A. and Aboulahris M. (2017) Modification of REE distribution of ordinary chondrites from Atacama (Chile)
935 and Lut (Iran) hot deserts: Insights into the chemical weathering of meteorites. *Meteorit. Planet. Sci.* **52**,
936 1843-1858.
- 937 Pourkhorsandi H., Gattacceca J., Rochette P., D'Orazio M., Kamali H., de Avillez R., Letichevsky S., Djamali
938 M., Mirnejad H., Debaille V. and Jull A.J.T. (2019) Meteorites from the Lut Desert (Iran). *Meteorit. Planet.*
939 *Sci.* **54**, 1737-1763.
- 940 Pourkhorsandi H., Debaille V., Armytage R. M. G., van Ginneken M., Rochette P. and Gattacceca J. (2021)
941 The effects of terrestrial weathering on samarium-neodymium isotopic composition of ordinary chondrites.

- 942 *Chem. Geol.* **562**, 120056.
- 943 Richter K. and Shearer C.K. (2003) Magmatic fractionation of Hf and W: Constraints on the timing of core
944 formation and differentiation in the Moon and Mars. *Geochim. Cosmochim. Acta* **67**, 2497-2507.
- 945 Shima M. (1979) The abundances of titanium, zirconium and hafnium in stony meteorites. *Geochim.*
946 *Cosmochim. Acta* **43**, 353-362.
- 947 Shima M. and Honda M. (1967) Distributions of alkali, alkaline earth and rare earth elements in component
948 minerals of chondrites. *Geochim. Cosmochim. Acta* **31**, 1995-2006.
- 949 Shimizu H., Masuda A. and Tanaka T. (1983) Cerium anomaly in REE pattern of Antarctic eucrite. *Mem. Nat.*
950 *Inst. Polar Res, Tokyo. Spec Issue* **30**, 341-348.
- 951 Shinotsuka K. (1997) Abundances of rare earth elements, thorium and uranium in chondritic meteorites. Ph.
952 D. Thesis, Tokyo Metropolitan University, Tokyo, Japan. DOI: 10.11501/3126008.
- 953 Stöffler D., Keil K. and Scott E. R. D. (1991) Shock metamorphism of ordinary chondrites. *Geochim.*
954 *Cosmochim. Acta* **55**, 3845-3867.
- 955 Su N., Yang S. Y., Guo Y. L., Yue W., Wang X. D., Yin P. and Huang X. T. (2017) Revisit of rare earth
956 element fractionation during chemical weathering and river sediment transport. *Geochem. Geophys. Geosyst.*
957 **18**, 935-955.
- 958 Tatsumoto M., Knight R. J. and Allegre C. J. (1973) Time Differences in the Formation of Meteorites as
959 Determined from the Ratio of Lead-207 to Lead-206. *Science* **180**, 1279-1283.
- 960 Tatsumoto M., Unruh D. M. and Patchett P. J. (1981) U-Pb and Lu-Hf systematics of Antarctic meteorites.
961 *Mem. Nat. Inst. Polar Res, Tokyo. Spec Issue* **20**, 237-249.
- 962 Taylor S. R. and McLennan S. M. (1995) The geochemical evolution of the continental crust. *Rev. Geophys.*
963 **33**, 241-265.
- 964 van der Weijden C. H. and van der Weijden R. D. (1995) Mobility of major, minor and some redox-sensitive
965 trace elements and rare-earth elements during weathering of four granitoids in central Portugal. *Chem. Geol.*
966 **125**, 149-167.
- 967 Van Schmus W. R. (1969) The mineralogy and petrology of chondritic meteorites. *Earth Sci. Rev.* **5**, 145-184.
- 968 Velbel M. A. (1988) The distribution and significance of evaporitic weathering products on Antarctic
969 meteorites. *Meteoritics* **23**, 151-159.
- 970 Velbel M. A., Long D. T. and Gooding J. L. (1991) Terrestrial weathering of Antarctic stone meteorites:
971 Formation of Mg-carbonates on ordinary chondrites. *Geochim. Cosmochim. Acta* **55**, 67-76.
- 972 Ward D., Bischoff A., Roszjar J. and Whitehouse M. J. (2017) Trace element inventory of meteoritic Ca-

973 phosphates. *American Mineralogist*, **102**, 1856-1880.

974 Wasson J. T. and Kallemeyn G. W. (1988) Compositions of chondrites. *Philos. Trans. R. Soc. Lond.*, A **325**,
975 535-544.

976 Weis D., Kieffer B., Maerschalk C., Barling J., de Jong J., Williams G. A., Hanano D., Pretorius W., Mattielli
977 N., Scoates J. S., Goolaerts A., Friedman R. M. and Mahoney J. B. (2006) High-precision isotopic
978 characterization of USGS reference materials by TIMS and MC-ICP-MS. *Geochem. Geophys. Geosyst.* **7**,
979 Q08006.

980 Weis D., Kieffer B., Hanano D., Silva I. N., Barling J., Pretorius W., Maerschalk C. and Mattielli N. (2007)
981 Hf isotope compositions of US Geological Survey reference materials. *Geochem. Geophys. Geosyst.* **8**,
982 Q06006.

983 Weisberg M. K., Prinz M., Clayton R. N., Mayeda T. K., Grady M. M., Franchi I., Pillinger C. T. and
984 Kallemeyn G. W. (1996) The K (Kakangari) chondrite grouplet. *Geochim. Cosmochim. Acta* **60**, 4253–4263.

985 Welten K. C., Nishiizumi K., Masarik J., Caffee M. W., Jull A. J. T., Klandrud S. E. And Wieler R. (2000)
986 Cosmic-ray exposure history of two Frontier Mountain H-chondrite showers from spallation and neutron-
987 capture products. *Meteorit. Planet. Sci.* **36**, 301-317.

988 Whillans I. M. and Cassidy W. A. (1983) Catch a falling star: Meteorites and old ice. *Science* **222**, 55-57.

989 de Winter N. J. and Claeys Ph. (2017) Micro X-ray fluorescence (μ XRF) line scanning on Cretaceous rudist
990 bivalves: A new method for reproducible trace element profiles in bivalve calcite. *Sedimentology* **64**, 231-
991 251.

992 Yamaguchi A., Shiraishi K. and Harvey R. (2021) The discovery of meteorites near the Yamato Mountains:
993 How the 1969 discoveries changed planetary science. *Meteorit. Planet. Sci.* **56**, 11-12.

994 Zanda B., Bourot-Denise M., Perron C. and Hewins R. H. (1994) Origin and metamorphic redistribution of
995 silicon, chromium and phosphorus in the metal of chondrites. *Science* **265**, 1846–1849.

996

997

998

999

1000

1001

1002

1003 **TABLE CAPTIONS**

1004 **Table 1.** List of H chondrites analyzed in this study.

1005 * The shock stages are estimated from descriptions of the shock degree in Meteorite Newsletter, NIPR,
1006 based on Stöffler *et al.* (1991).

1007 ^a Meteorite Newsletter, NIPR. ^b Antarctic Meteorite Newsletter, NASA.

Meteorite	Section Number		Type ^{a, b}	Weathering ^{a, b} index	Shock stage	Sources
	PTS	Powder				
A-881258	71-A	82	H3.0	B	?	NIPR
A-880941	51-A	48	H3.3	A/B	S1-2*	NIPR
Y-793574	51-A	56	H3.5	?	?	NIPR
Y-790461	91-A	100	H3.7	B	S3*	NIPR
ALH 78084	81-A	89	H3.9	B/Ce	?	NIPR
A 09436	-	-	H3	C	?	RBINS
A 09387	-	-	H4	B/C	?	RBINS
A 09618	-	-	H5	C	?	RBINS
A 09516	-	-	H6	C	?	RBINS
Y-790960	63-A	62	H7	B	S3*	NIPR
NWA 6752	-	-	H3	W2	S1	RBINS
NWA 6771	-	-	H4	W1	S1	RBINS
Sahara 97035	-	-	H5	W2	S1	RBINS

1008

1009 **Table 2.** Elemental abundances and isotope compositions in BHVO-2 (ID: isotope dilution, n.a.: not
1010 analyzed).

1011 The uncertainties of elemental abundances (1SD), ¹⁴³Nd/¹⁴⁴Nd, and ¹⁷⁶Hf/¹⁷⁷Hf (2SE) reflect internal
1012 reproducibilities during the measurements by ICP-OES, Q-ICP-MS, and MC-ICP-MS. The uncertainties of
1013 the elemental abundances (ID), ¹⁴⁷Sm/¹⁴⁴Nd, and ¹⁷⁶Lu/¹⁷⁷Hf (2SE) reflect the maximum uncertainties due to
1014 spike calibrations (see subsection 2.3.2).

1015 * The uncertainty of the ¹⁷⁶Hf/¹⁷⁷Hf value (2SE) reflects external reproducibilities during the measurements
1016 of MC-ICP-MS.

1017 ^a Jochum *et al.* (2016) for elemental abundances including those determined by isotope dilution, ¹⁴⁷Sm/¹⁴⁴Nd,
1018 and ¹⁷⁶Lu/¹⁷⁷Hf. ^b Weis *et al.* (2006) for ¹⁴³Nd/¹⁴⁴Nd. ^c Weis *et al.* (2007) for ¹⁷⁶Hf/¹⁷⁷Hf.

	This work		Preferred values ^{a-c}
(%)			
Na	1.79 ± 0.00	1.59 ± 0.02	1.646 ± 0.036
Mg	4.74 ± 0.03	4.44 ± 0.02	4.376 ± 0.025
Al	7.79 ± 0.05	6.87 ± 0.03	7.113 ± 0.032
P	0.115 ± 0.002	0.114 ± 0.003	0.1172 ± 0.0022
K	0.439 ± 0.005	0.416 ± 0.001	0.4259 ± 0.0031
Ca	8.15 ± 0.02	7.66 ± 0.03	8.148 ± 0.043
Ti	1.68 ± 0.01	1.57 ± 0.00	1.637 ± 0.011
Cr	0.0310 ± 0.0008	0.0335 ± 0.0004	0.02872 ± 0.00031
Mn	0.129 ± 0.002	0.130 ± 0.002	0.1309 ± 0.0015
Fe	8.73 ± 0.01	8.30 ± 0.01	8.666 ± 0.063
(ppm)			
Ni	127 ± 31	127 ± 4	119.8 ± 1.2
Co	80.8 ± 1.7	76.5 ± 1.9	44.89 ± 0.32
Cu	123 ± 1	119 ± 1	129.3 ± 1.4
Zn	97.9 ± 0.5	123 ± 1	103.9 ± 1.0
Rb	9.91 ± 0.10	8.24 ± 0.19	9.261 ± 0.096
Sr	370 ± 2	354 ± 5	394.1 ± 1.7
Y	25.7 ± 0.1	24.3 ± 0.2	25.91 ± 0.28
Zr	165 ± 1	157 ± 1	171.2 ± 1.3
Nb	16.9 ± 0.1	16.4 ± 0.1	18.10 ± 0.20
Ba	126 ± 1	121 ± 2	130.9 ± 1.0
La	15.7 ± 0.2	15.2 ± 0.2	15.20 ± 0.08
Ce	37.7 ± 0.4	36.5 ± 0.5	37.53 ± 0.19
Pr	5.20 ± 0.03	5.08 ± 0.08	5.339 ± 0.028
Nd	24.7 ± 0.2	23.7 ± 0.4	24.27 ± 0.25
Sm	6.01 ± 0.13	5.75 ± 0.1	6.023 ± 0.057
Eu	2.02 ± 0.03	1.98 ± 0.03	2.043 ± 0.012
Gd	6.47 ± 0.11	6.18 ± 0.12	6.207 ± 0.038
Tb	0.914 ± 0.012	0.876 ± 0.020	0.9392 ± 0.0053
Dy	5.29 ± 0.05	5.11 ± 0.08	5.280 ± 0.028
Ho	0.980 ± 0.015	0.940 ± 0.020	0.9887 ± 0.0053
Er	2.57 ± 0.03	2.43 ± 0.04	2.511 ± 0.014
Tm	0.335 ± 0.004	0.315 ± 0.012	0.3349 ± 0.0031
Yb	2.00 ± 0.06	1.93 ± 0.01	1.994 ± 0.027
Lu	0.278 ± 0.005	0.256 ± 0.008	0.2754 ± 0.0024
Hf	4.40 ± 0.04	4.06 ± 0.12	4.470 ± 0.025
Th	1.38 ± 0.06	1.14 ± 0.05	1.224 ± 0.016
U	0.412 ± 0.007	0.377 ± 0.012	0.412 ± 0.035
Nd (ID)		22.5 ± 0.1	24.27 ± 0.18
Sm (ID)		5.63 ± 0.03	6.023 ± 0.038
Lu (ID)	n.a.	0.249 ± 0.001	0.2754 ± 0.0018
Hf (ID)		4.04 ± 0.02	4.470 ± 0.020

1020 **Table 3.** Modal abundances in H chondrites: vol. % at left; wt. % at right (UHC: unequilibrated H chondrite, EHC: equilibrated H chondrite).
1021 Wt. % is calculated from vol. % using the following estimated mineral specific gravities and normalized to 100%: olivine (3.48), low-Ca pyroxene (3.2). Ca-pyroxene (3.4),
1022 feldspar (2.62), kamacite (7.9), taenite (8.01), troilite (4.61), chlorapatite (3.16), merrillite (3.12), chromite (4.6).
1023 The uncertainties for the mean values from this study are 95% confidence interval, and those for McSween *et al.*, (1991) are 2SE calculated from their data.
1024 * The modal abundances of low-Ca pyroxene, feldspar, and chromite obtained in this study may include forsterite, silica, and ilmenite, respectively (see section 3.1).

Name	A-881258		A-880941		Y-793574		Y-790461		ALH 78084		A 09436		A 09387		A 09618		A 09516		Y-790960	
Area (mm ²)	71.294		52.706		61.594		104.907		81.524		190.921		89.756		152.775		177.284		34.607	
Olivine	40.7	38.9	36.8	33.4	34.4	32.2	38.0	35.9	35.8	33.5	35.4	33.1	36.8	35.4	38.0	35.6	36.8	33.4	38.7	36.0
Low-Ca pyroxene*	30.7	27	24.1	20	27.4	24	26.8	23	29.7	26	32.8	28	29.2	26	30.6	26	30.8	26	29.0	25
Ca-pyroxene	1.15	1.1	6.26	5.6	7.88	7.2	5.53	5.1	5.51	5.0	4.52	4.1	4.86	4.6	2.26	2.1	3.94	3.5	5.02	4.6
Feldspar*	14.8	10.7	14.5	9.91	14.6	10.3	14.7	10.5	14.1	9.91	13.1	9.22	14.3	10.3	13.6	9.58	10.9	7.45	14.0	9.77
Kamacite	6.01	13	3.52	7.2	5.76	12	6.05	13	6.64	14	6.09	13	4.81	10	7.23	15	7.35	15	6.46	14
Taenite	1.59	3.49	8.85	18.5	3.49	7.51	2.67	5.82	2.86	6.17	3.15	6.76	2.91	6.44	2.06	4.45	4.40	9.19	2.59	5.54
Troilite	3.59	4.55	3.12	3.75	4.33	5.36	3.93	4.92	3.47	4.30	3.74	4.62	4.04	5.15	3.97	4.94	3.50	4.20	3.79	4.67
Chlorapatite	0.05	0.04	0.09	0.07	0.11	0.10	0.05	0.04	0.29	0.25	0.16	0.14	0.03	0.02	0.30	0.26	0.14	0.11	0.35	0.30
Merrillite	0.47	0.41	0.37	0.30	0.38	0.32	0.41	0.35	0.32	0.27	0.36	0.30	0.90	0.78	0.33	0.28	0.78	0.64	0.43	0.36
Total Ca-phosphates	0.52	0.45	0.46	0.38	0.49	0.41	0.46	0.39	0.61	0.51	0.52	0.44	0.93	0.80	0.63	0.53	0.92	0.75	0.78	0.66
Chromite*	0.59	0.74	0.97	1.2	1.05	1.3	0.81	1.0	0.72	0.89	0.60	0.74	0.77	0.97	0.79	0.98	0.63	0.76	0.28	0.35
Iron oxide	-	-	trace	-	trace	-	-	-	trace	-	trace	-	-	-	-	-	-	-	-	-
Silica	-	-	-	-	-	-	trace	-	-	-	-	-	trace	-	-	-	-	-	-	-
(Mg, Fe)-spinel	-	-	trace	-	-	-	trace	-	-	-	-	-	-	-	-	-	-	-	-	-
Hibonite	-	-	-	-	-	-	trace	-	-	-	-	-	-	-	-	-	-	-	-	-
(Zn, Fe)S	-	-	-	-	-	-	-	-	-	-	-	trace	trace	-	-	-	-	-	-	-

Total	99.6	98.6	99.3	99.0	99.3	100.0	98.6	99.0	99.3	100.7
-------	------	------	------	------	------	-------	------	------	------	-------

1025

1026 (continued)

Name	NWA 6752		NWA 6771		Sahara 97035		UHC mean (this study)		EHC mean (this study)		EHC mean (literature data; in wt. %)					
	Area (mm ²)/ n / Ref.		496.441		94.315		100.041		n = 7		n = 6		Van Schmus (1969)	McSween <i>et al.</i> (1991), n = 25		
Olivine	38.0	34.5	39.3	36.4	35.3	33.7	37.0 ± 1.9		34.5 ± 2.4		37.5 ± 1.5		35.1 ± 1.3		33 - 37	35.7 ± 1.5
Low-Ca pyroxene*	31.2	26	26.4	22	30.1	26	29.0 ± 2.8		25 ± 3		29.4 ± 1.7		25 ± 2		23 - 27	26.3 ± 1.2
Ca-pyroxene	2.02	1.8	5.55	5.0	5.50	5.1	4.70 ± 2.19		4.3 ± 2.0		4.52 ± 1.31		4.1 ± 1.2		4 - 5	4.1 ± 0.2
Feldspar*	9.00	6.15	12.1	8.40	13.8	9.89	13.5 ± 1.9		9.52 ± 0.58		13.1 ± 1.4		9.24 ± 1.14		9 - 10	9.6 ± 0.2
Kamacite	7.30	15	7.21	15	6.88	15	5.91 ± 1.09		13 ± 3		6.65 ± 1.01		14 ± 2		15 - 17	18.2 ± 0.6
Taenite	4.54	9.48	2.88	6.13	1.51	3.32	3.88 ± 2.19		8.25 ± 4.64		2.72 ± 1.03		5.84 ± 2.10		2 - 3	
Troilite	4.88	5.86	3.95	4.85	4.06	5.14	3.86 ± 0.54		4.77 ± 0.47		3.89 ± 0.22		4.82 ± 0.37		5 - 6	5.5 ± 0.2
Chlorapatite	0.06	0.05	0.42	0.35	trace		0.12 ± 0.08		0.10 ± 0.07		0.21 ± 0.17		0.17 ± 0.14		-	-
Merrillite	0.14	0.12	0.41	0.34	0.89	0.76	0.35 ± 0.10		0.29 ± 0.08		0.62 ± 0.27		0.53 ± 0.24		-	-
Total Ca-phosphates	0.20	0.17	0.83	0.69	0.89	0.76	0.47 ± 0.12		0.39 ± 0.09		0.83 ± 0.12		0.70 ± 0.10		0.6	0.65 ± 0.03
Chromite*	0.83	0.99	0.80	0.98	0.48	0.60	0.79 ± 0.16		0.98 ± 0.20		0.63 ± 0.22		0.77 ± 0.27		0.5	0.76 ± 0.02
Iron oxide	trace		-		-											
Silica	-		-		-											
(Mg, Fe)-spinel	-		-		-											
Hibonite	-		-		-											
(Zn, Fe)S	-		-		-											
Total	98.0		98.9		98.5											

1027

1028 **Table 4.** Elemental abundances and isotope compositions in H chondrites (UHC: unequilibrated H chondrite,
1029 EHC: equilibrated H chondrite, ID: isotope dilution, n.d.: not determined).
1030 The uncertainties for each sample reflect the same as those in Table 2 and the number of digits is based on
1031 the reproducibility of the reference material. The uncertainties for the mean values are 95% confidence
1032 interval. The elemental abundances (ID) and the isotope ratios for non-Antarctic HC are mean values of H
1033 chondrite falls from the following literatures (see Supplementary data).
1034 * The data of A 09516 (H6) are excluded from the means (see section 3.2).
1035 ^a Jarosewich (1990) for Na-Ni. ^b Wasson and Kallemeyn (1988) for Cu-Ba and Hf. ^c Nakamura (1974) for
1036 REEs. ^d Tatsumoto *et al.* (1973) for Th and U. ^e Jacobsen and Wasserburg (1980, 1984), Patchett *et al.*
1037 (2004), Boyet and Carlson (2005), Carlson *et al.* (2007), Bouvier *et al.* (2008), Gannoun *et al.* (2011),
1038 Burkhardt *et al.* (2016), and Fukai and Yokoyama (2017) for Nd and Sm isotope compositions. ^f Blichert-
1039 Toft and Albarède (1997), Bizzarro *et al.* (2003), Patchett *et al.* (2004), Bouvier *et al.* (2008), and Dauphas
1040 and Pourmand (2011) for Lu and Hf isotope compositions.

1041

Name	A-881258	A-880941	Y-793574	Y-790461	ALH 78084
(%)					
Na	0.56 ± 0.03	0.54 ± 0.04	0.68 ± 0.04	0.61 ± 0.01	0.62 ± 0.03
Mg	14 ± 0	13 ± 0	15 ± 0	14 ± 0	14 ± 0
Al	0.99 ± 0.00	0.92 ± 0.00	1.1 ± 0.0	1.1 ± 0.0	1.0 ± 0.00
P	0.11 ± 0.00	0.11 ± 0.00	0.13 ± 0.00	0.12 ± 0.00	0.10 ± 0.00
K	0.065 ± 0.001	0.050 ± 0.001	0.071 ± 0.002	0.065 ± 0.002	0.065 ± 0.001
Ca	0.98 ± 0.00	0.94 ± 0.01	1.2 ± 0.0	1.0 ± 0.0	1.0 ± 0.0
Ti	0.057 ± 0.01	0.050 ± 0.002	0.061 ± 0.002	0.062 ± 0.001	0.055 ± 0.000
Cr	0.38 ± 0.00	0.34 ± 0.00	0.41 ± 0.00	0.40 ± 0.00	0.35 ± 0.00
Mn	0.23 ± 0.00	0.22 ± 0.00	0.25 ± 0.00	0.23 ± 0.00	0.23 ± 0.00
Fe	23 ± 1	22 ± 0	27 ± 0	23 ± 0	22 ± 0
Ni	1.6 ± 0.0	1.6 ± 0.0	1.6 ± 0.1	1.5 ± 0	1.5 ± 0.0
Co	0.064 ± 0.001	0.066 ± 0.000	0.085 ± 0.001	0.060 ± 0.000	0.065 ± 0.01
(ppm)					
Cu	88.0 ± 0.6	80.0 ± 1.6	78.0 ± 1.4	90.5 ± 1.8	75.2 ± 1.7
Zn	63.9 ± 0.8	52.1 ± 1.3	61.4 ± 0.9	61.2 ± 0.7	54.8 ± 1.3
Rb	2.45 ± 0.08	1.29 ± 0.05	2.29 ± 0.05	2.67 ± 0.07	2.26 ± 0.08
Sr	8.77 ± 0.13	8.76 ± 0.14	8.53 ± 0.14	9.42 ± 0.12	8.66 ± 0.23
Y	1.90 ± 0.02	1.97 ± 0.06	1.87 ± 0.04	1.98 ± 0.05	2.08 ± 0.05
Zr	4.78 ± 0.08	4.79 ± 0.10	4.69 ± 0.08	5.28 ± 0.09	5.31 ± 0.02
Nb	0.358 ± 0.014	0.356 ± 0.008	0.375 ± 0.007	0.370 ± 0.015	0.382 ± 0.008
Ba	3.19 ± 0.07	3.17 ± 0.07	3.06 ± 0.01	3.38 ± 0.02	3.18 ± 0.02

(ppb)					
La	299 ± 10	330 ± 8	324 ± 4	333 ± 10	317 ± 15
Ce	788 ± 19	833 ± 24	830 ± 21	850 ± 22	820 ± 40
Pr	116 ± 4	121 ± 8	119 ± 2	125 ± 4	113 ± 2
Nd	549 ± 19	602 ± 53	618 ± 14	581 ± 42	615 ± 60
Sm	177 ± 15	216 ± 12	181 ± 6	208 ± 12	188 ± 18
Eu	72.9 ± 3.4	73.8 ± 4.8	74.3 ± 3.0	76.6 ± 5.4	65.3 ± 4.8
Gd	257 ± 15	283 ± 17	292 ± 8	289 ± 19	285 ± 17
Tb	45.1 ± 2.7	47.2 ± 3.2	49.8 ± 0.9	46.9 ± 2.6	47.5 ± 2.5
Dy	324 ± 8	335 ± 11	337 ± 17	338 ± 20	365 ± 15
Ho	67.5 ± 3.0	75.0 ± 2.7	75.8 ± 1.5	74.3 ± 2.6	77.6 ± 2.3
Er	206 ± 3	215 ± 9	226 ± 7	232 ± 3	229 ± 4
Tm	30.2 ± 0.7	32.1 ± 1.7	34.6 ± 2.0	32.3 ± 1.4	31.5 ± 1.6
Yb	210 ± 12	210 ± 5	226 ± 8	211 ± 13	220 ± 9
Lu	30.1 ± 3.1	31.7 ± 4.3	34.3 ± 2.1	32.8 ± 2.7	30.0 ± 0.6
Hf	123 ± 9	135 ± 3	140 ± 10	147 ± 14	149 ± 7
Th	42.7 ± 1.4	38.1 ± 0.9	42.4 ± 0.6	43.0 ± 2.5	39.7 ± 1.9
U	11.4 ± 1.1	9.99 ± 0.64	12.4 ± 0.4	10.8 ± 0.5	12.0 ± 0.7
Nd (ID)	585 ± 3	609 ± 3	527 ± 3	604 ± 3	543 ± 3
Sm (ID)	190 ± 1	196 ± 1	172 ± 1	197 ± 1	178 ± 1
Lu (ID)	28.9 ± 0.1	29.7 ± 0.1	32.4 ± 0.2	29.2 ± 0.1	31.0 ± 0.2
Hf (ID)	123 ± 1	125 ± 1	152 ± 1	136 ± 1	140 ± 1
¹⁴⁷ Sm/ ¹⁴⁴ Nd	0.1958 ± 0.0014	0.1949 ± 0.0014	0.1977 ± 0.0014	0.1971 ± 0.0014	0.1986 ± 0.0014
¹⁴³ Nd/ ¹⁴⁴ Nd	0.512604 ± 0.000007	0.512570 ± 0.000014	0.512712 ± 0.000009	0.512585 ± 0.000008	0.512619 ± 0.000008
¹⁷⁶ Lu/ ¹⁷⁷ Hf	0.0336 ± 0.0002	0.0338 ± 0.0002	0.0304 ± 0.0002	0.0306 ± 0.0002	0.0315 ± 0.0002
¹⁷⁶ Hf/ ¹⁷⁷ Hf	0.282825 ± 0.000015	0.282868 ± 0.000016	0.282825 ± 0.000038	0.282689 ± 0.000019	0.282702 ± 0.000013

1043 **Table 5.** Elemental abundance ratios in H chondrites (UHC: unequilibrated H chondrite, EHC: equilibrated
 1044 H chondrite).

1045 The uncertainties are derived from the uncertainties of the respective elemental abundances. The
 1046 uncertainties for the mean values are 95% confidence interval. The mean values of non-Antarctic HC and
 1047 Antarctic HC are calculated from the following literatures.

1048 * The data of A 09516 (H6) are excluded from the means (see section 3.2).

1049 ^a Jarosewich (1990) for Na and Al. ^b Wasson and Kallemeyn (1988) for Rb, Sr, and Ba. ^c Nishikawa *et al.*,
 1050 (1990) for Rb, Sr, and Ba.

Name	Rb	Sr	Ba
	(Na + Al)/2	(Na + Al)/2	(Na + Al)/2
A-881258	3.16 ± 0.12	11.3 ± 0.3	4.11 ± 0.14
A-880941	1.77 ± 0.09	12.0 ± 0.5	4.35 ± 0.18
Y-793574	2.56 ± 0.09	9.55 ± 0.32	3.43 ± 0.15
Y-790461	3.19 ± 0.09	11.3 ± 0.2	4.04 ± 0.24
ALH 78084	2.80 ± 0.13	10.7 ± 0.4	3.94 ± 0.24
A 09436-1	2.32 ± 0.05	10.7 ± 0.2	4.04 ± 0.15
A 09436-2	2.38 ± 0.07	11.1 ± 0.2	4.23 ± 0.11
A 09387	3.77 ± 0.11	10.7 ± 0.3	3.88 ± 0.11
A 09618	2.65 ± 0.06	11.0 ± 0.2	3.96 ± 0.08
A 09516-1	0.895 ± 0.049	8.71 ± 0.35	3.19 ± 0.15
A 09516-2	1.29 ± 0.07	12.3 ± 0.5	5.24 ± 0.31
Y-790960	3.11 ± 0.22	10.4 ± 0.3	3.65 ± 0.25
NWA 6752	2.51 ± 0.09	26.5 ± 0.7	202 ± 6
NWA 6771	3.21 ± 0.08	21.8 ± 0.5	22.9 ± 0.5
Sahara 97035	3.96 ± 0.13	123 ± 3	51.4 ± 1.3
Antarctic UHC mean (n = 7)	2.60 ± 0.50	11.0 ± 0.8	4.02 ± 0.29
Antarctic EHC mean* (n = 3)	3.17 ± 0.56	10.7 ± 0.3	3.83 ± 0.16
Antarctic HC mean* (n = 10)	2.77 ± 0.56	10.9 ± 0.7	3.96 ± 0.27
Hot desert HC mean (n = 3)	3.23 ± 3.23	57.2 ± 57.4	92.1 ± 96.3
Non-Antarctic HC mean ^{a, b}	3.28 ± 0.09	11.3 ± 0.3	4.74 ± 0.13
Antarctic HC mean ^{a, c}	3.24 ± 0.48	10.5 ± 1.1	3.04 ± 0.85

1051

1052

1053

1054

1055

1056

1057

1058

1059

1060 **Table 6.** Correlation coefficients (r) between elemental ratios and isotopic ratios in Antarctic HCs.
 1061 Strong and no correlations are defined as $|r| > 0.6$ and $0.4 > |r|$, and are shown in bolded and underlined,
 1062 respectively.

	Correlation coefficients for all samples				Correlation coefficients excluding A 09516 (H6)			
	$^{147}\text{Sm}/^{144}\text{Nd}$	$^{143}\text{Nd}/^{144}\text{Nd}$	$^{176}\text{Lu}/^{177}\text{Hf}$	$^{176}\text{Hf}/^{177}\text{Hf}$	$^{147}\text{Sm}/^{144}\text{Nd}$	$^{143}\text{Nd}/^{144}\text{Nd}$	$^{176}\text{Lu}/^{177}\text{Hf}$	$^{176}\text{Hf}/^{177}\text{Hf}$
Al/Mg	-0.50	<u>0.29</u>	-0.42	<u>-0.12</u>	<u>-0.21</u>	-0.47	<u>-0.36</u>	-0.51
P/Mg	0.48	-0.57	0.64	0.62	-0.60	-0.45	<u>-0.04</u>	<u>0.09</u>
Ca/Mg	<u>0.19</u>	0.40	<u>-0.24</u>	<u>-0.01</u>	<u>0.14</u>	0.45	-0.74	-0.54
Ti/Mg	-0.42	<u>0.28</u>	-0.63	-0.43	<u>-0.23</u>	<u>-0.01</u>	-0.79	-0.73
Y/Mg	0.65	-0.65	0.78	0.66	<u>0.04</u>	-0.48	0.56	0.40
P/Ca	<u>0.33</u>	-0.74	0.74	0.60	-0.47	-0.63	0.58	0.50
Y/Ca	0.41	-0.71	0.75	0.49	<u>-0.06</u>	-0.55	0.80	0.58

1063

1064

1065

1066

1067 **Table 7.** Major hosts of REEs and Hf, and alteration types for chondrites.

1068 ^a Curtis and Schmitt (1979) and Ebihara and Honda (1983). ^b Larimer and Ganapathy (1987) and Ebihara
 1069 (1988). ^c Martin *et al.* (2013). ^d Ebihara and Honda (1987). ^e Maeda *et al.* (2017a, 2017b). ^f Alexander
 1070 (1994) and Mason and Graham (1970). ^g Barrat *et al.* (2014). ^h Krot *et al.* (2003) and Huss *et al.* (2006). ⁱ
 1071 Weisberg *et al.* (1996) and Barosch *et al.* (2020).

Chondrite	Major hosts of REEs	Major hosts of Hf	Alteration type
H, L, LL	Ca-phosphates ^a	Ca-pyroxene (silicates) ^f	
EH, EL	Oldhamite (CaS) ^b	Sulfides and silicates ^g	Thermal metamorphism ^h
CK	Ca-phosphates and silicates ^c	Silicates ^e	
CV	Ca, Al-rich inclusions (CAIs) ^d	?	Aqueous alteration and
CO	?	?	weak thermal metamorphism ^h
CI, CM, CR, CH, CB	?	?	Aqueous alteration ^h
Rumuruti	Ca-phosphates ^e	?	Thermal metamorphism ^h
Kakangari	?	?	Aqueous alteration and weak thermal metamorphism ⁱ

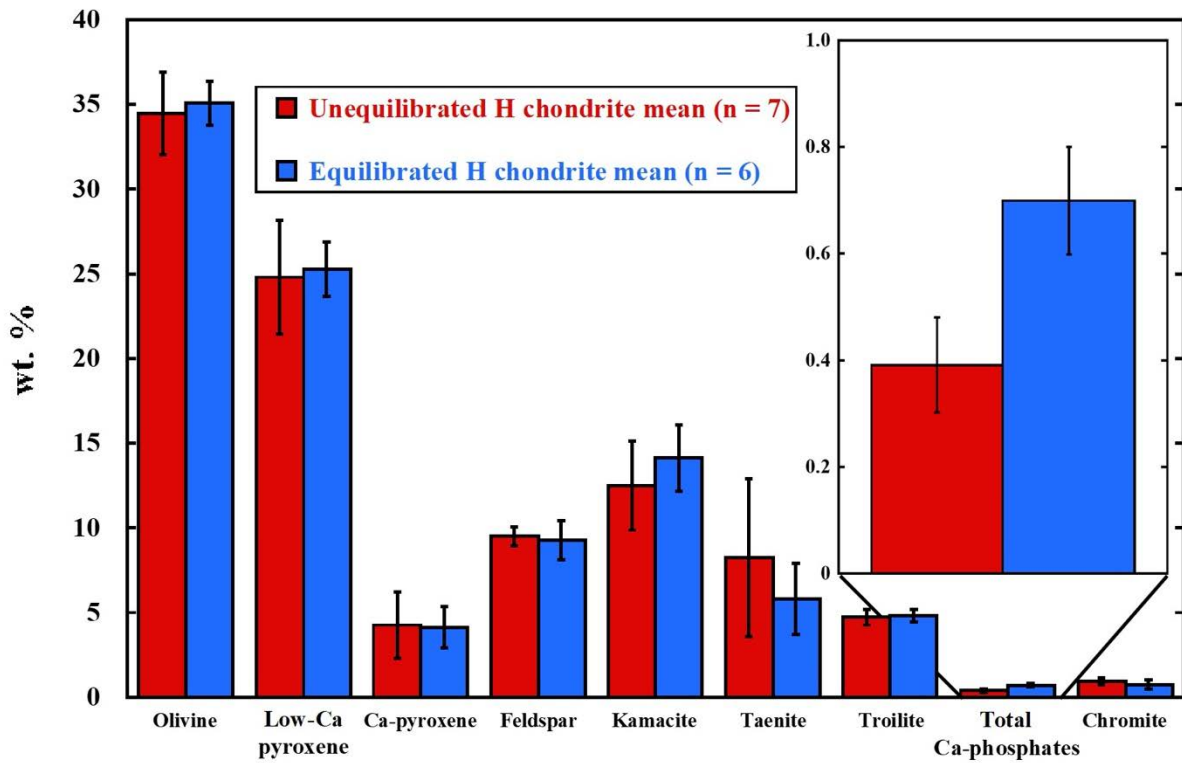
1072

1073

1074

1075 **FIGURE CAPTIONS**

1076 **Fig. 1.** The mean modal abundances (wt. %) in UHC and EHC obtained in this study (n = 7 and 6,
 1077 respectively). The mean modal abundances of low-Ca pyroxene, feldspar, and chromite may include forsterite,
 1078 silica, and ilmenite, respectively (see section 3.1). The uncertainties represent 95% confidence interval of the
 1079 mean values.



1080

1081

1082

1083

1084

1085

1086

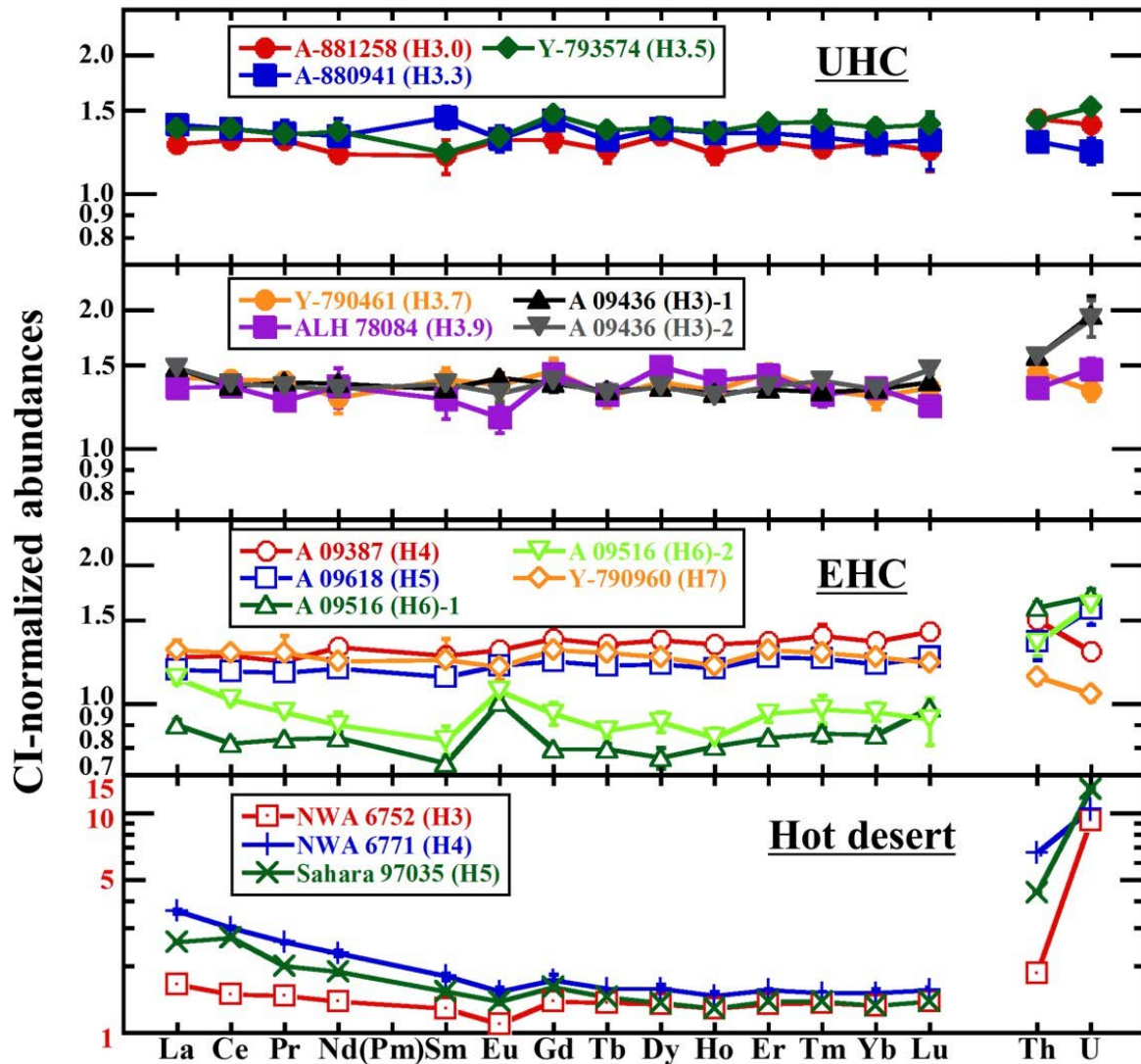
1087

1088

1089

1090

1091 **Fig. 2.** CI-normalized REE, Th, and U abundances in each Antarctic and hot desert HC. The uncertainties
 1092 represent 1SD of the measurements by Q-ICP-MS. Error bars are often smaller than the symbol size. Note
 1093 that the scale of y-axis for hot desert is different from the other. CI values are from Anders and Grevesse
 1094 (1989).



1095

1096

1097

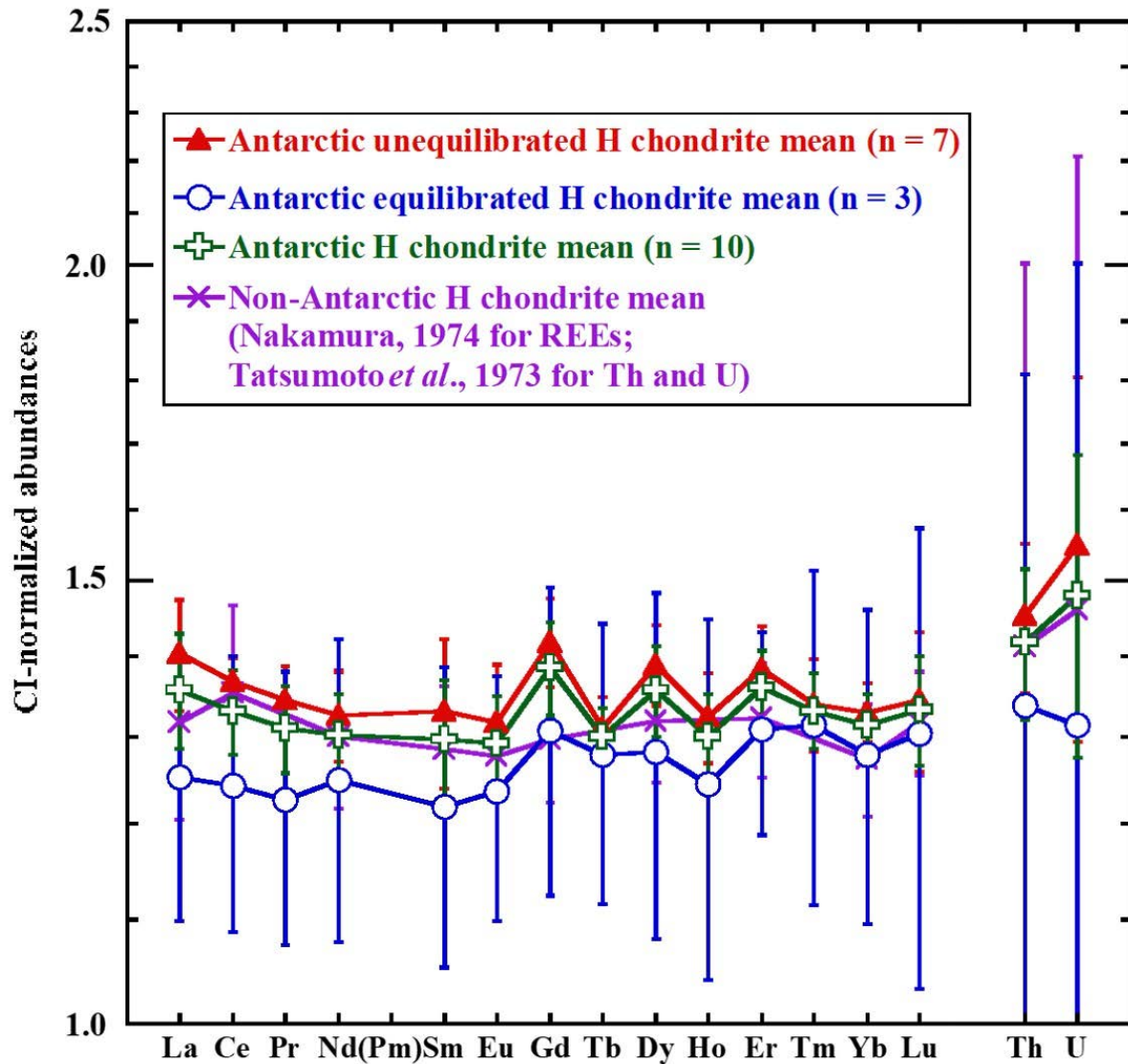
1098

1099

1100

1101

1102 **Fig. 3.** Mean CI-normalized REE, Th, and U abundances of Antarctic UHCs, Antarctic EHCs, and Antarctic
 1103 HCs (n = 7, 3, and 10, respectively). The mean values of non-Antarctic HCs are also shown for comparison
 1104 (Nakamura, 1974 for REEs; Tatsumoto et al., 1973 for Th and U). The uncertainties are 95% confidence
 1105 interval of the mean values. CI values from Anders and Grevesse (1989).



1106

1107

1108

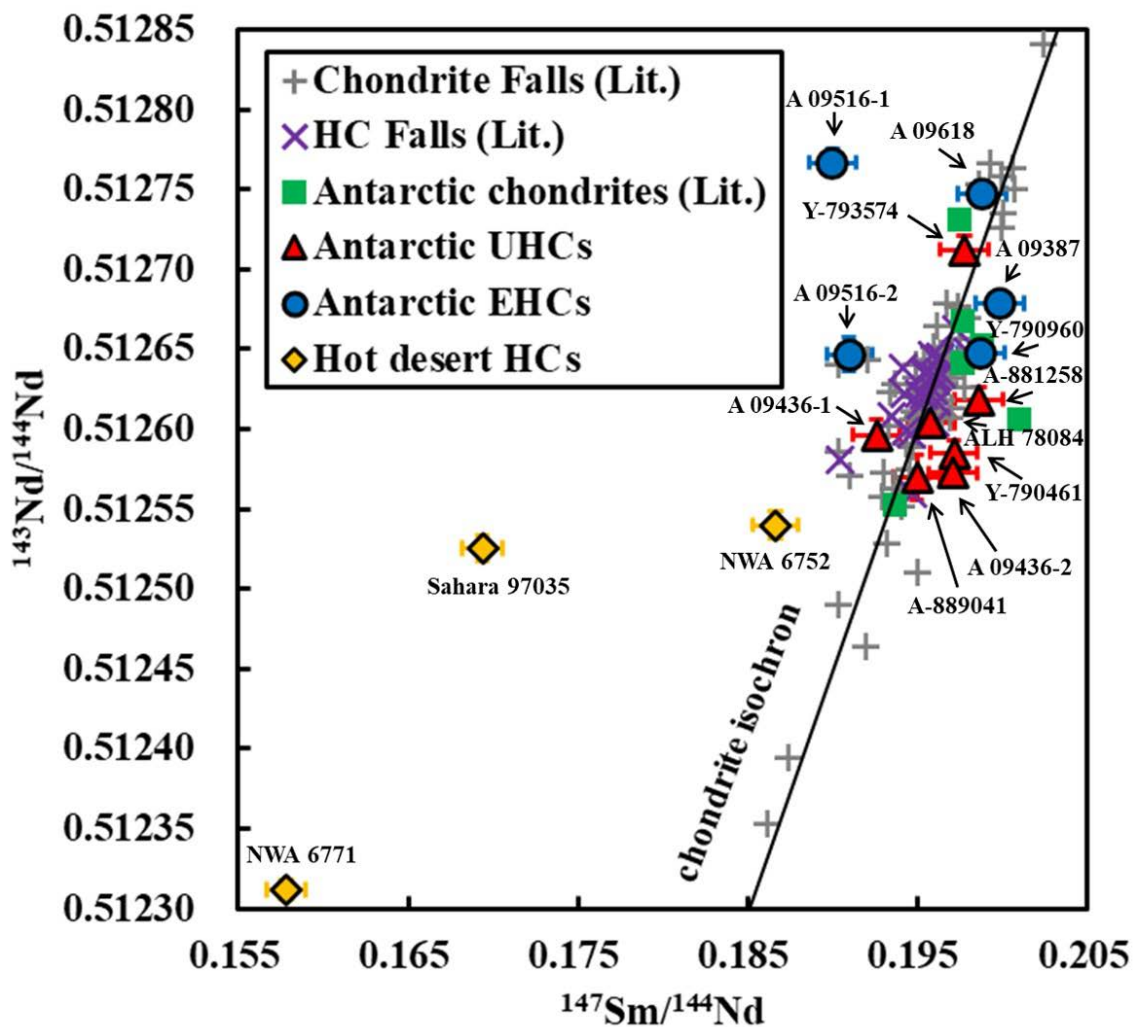
1109

1110

1111

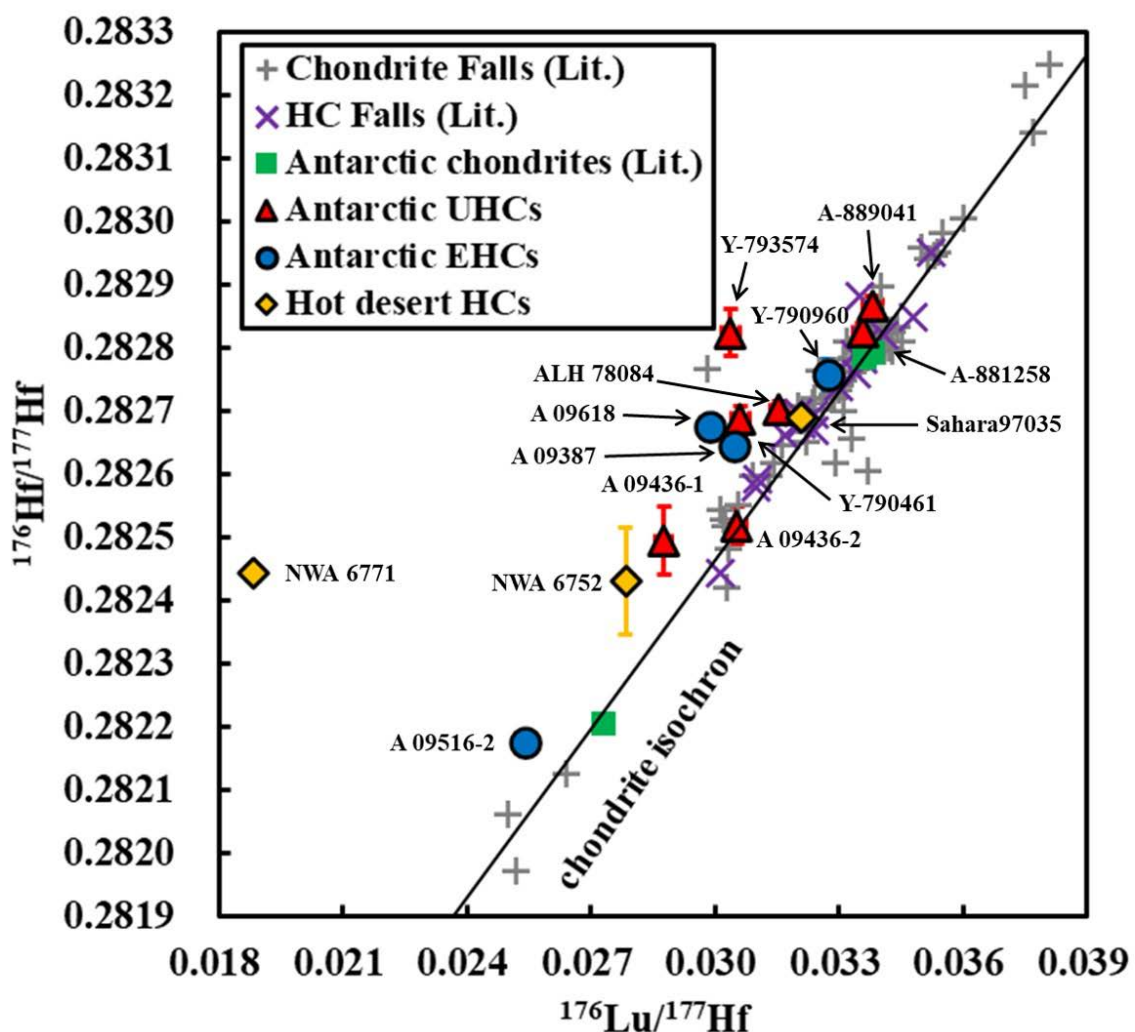
1112

1113 **Fig. 4.** Sm-Nd isotopic compositions of Antarctic UHCs, Antarctic EHCs, and HCs collected from hot deserts.
 1114 The isotope compositions of chondrite falls, HC falls, and Antarctic chondrites from literatures are shown for
 1115 comparison (Jacobsen and Wasserburg, 1980, 1984; Patchett *et al.*, 2004; Boyet and Carlson, 2005; Carlson
 1116 *et al.*, 2007; Bouvier *et al.*, 2008; Gannoun *et al.*, 2011; Burkhardt *et al.*, 2016; Fukai and Yokoyama, 2017;
 1117 see Supplementary data for the details). The uncertainties for the $^{143}\text{Nd}/^{144}\text{Nd}$ values are 2SE of the internal
 1118 reproducibility, and the uncertainties for the $^{147}\text{Sm}/^{144}\text{Nd}$ are 2SE of the total uncertainty derived from the
 1119 uncertainty of the spike calibration (see subsection 2.3.2). Error bars are often smaller than the symbol size.
 1120 The analytical uncertainties for the literature data are not shown. The chondrite isochron is from Bouvier *et al.*
 1121 *al.* (2008).



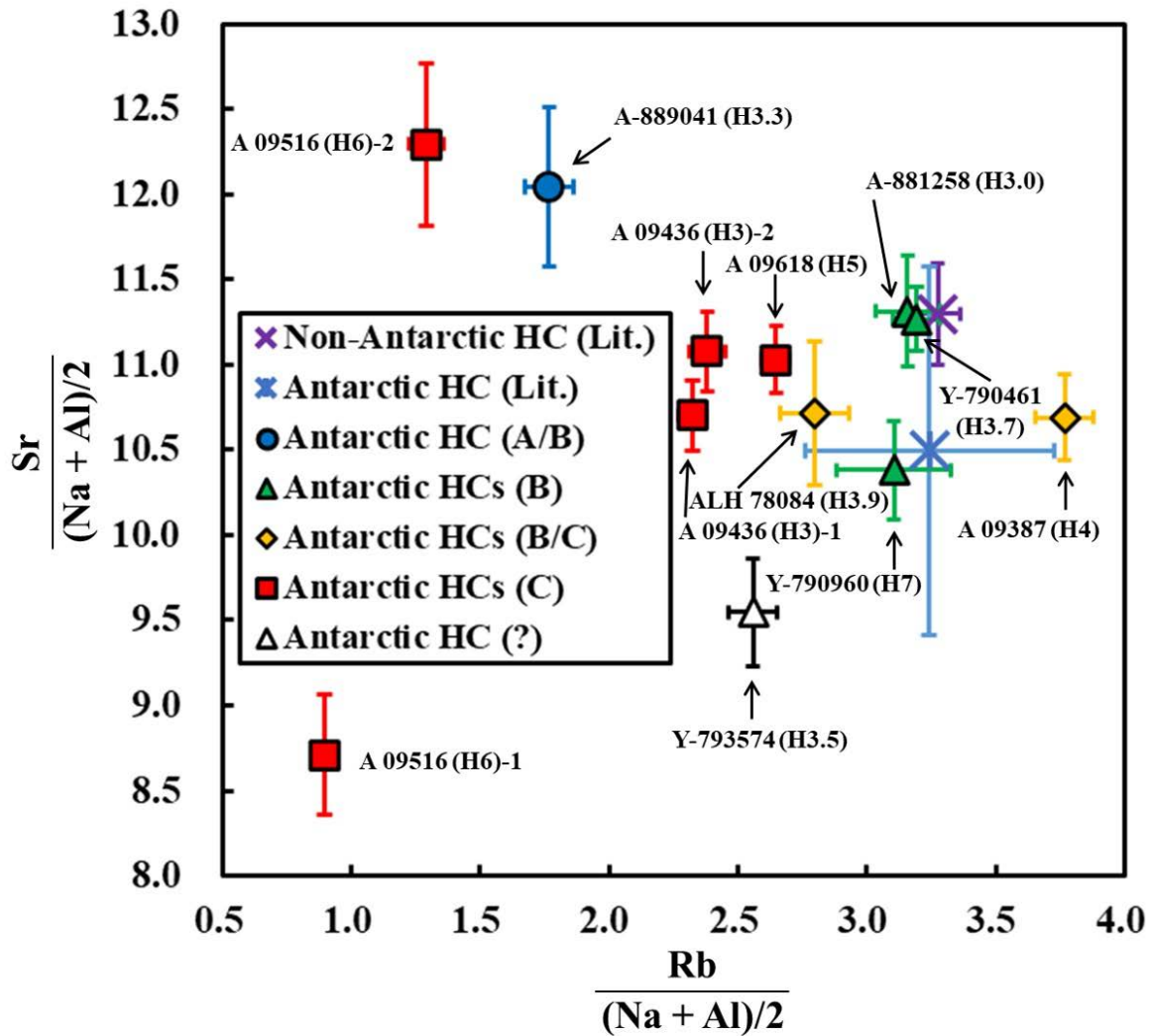
1122
 1123
 1124
 1125
 1126

1127 **Fig. 5.** Lu-Hf isotopic compositions of Antarctic UHCs, Antarctic EHCs, and HCs collected from hot deserts.
 1128 The isotope compositions of chondrite falls, HC falls, and Antarctic chondrites from literature are also shown
 1129 for comparison (Blichert-Toft and Albarède, 1997; Bizzarro *et al.*, 2003; Patchett *et al.*, 2004; Bouvier *et al.*,
 1130 2008; Dauphas and Pourmand, 2011; see Supplementary data for the details). Note that Blichert-Toft and
 1131 Albarède (1997) did not use high-pressure vessels during the sample digestion. The data of Farmington (L5),
 1132 Adhi Kot (EH4), and Jajh Deh Kot Lalu (EL6) from Dauphas and Pourmand (2011) plot outside the range of
 1133 the figure. The uncertainties for the $^{176}\text{Hf}/^{177}\text{Hf}$ values are 2SE of the internal reproducibility, and the
 1134 uncertainties for the $^{176}\text{Lu}/^{177}\text{Hf}$ values are 2SE of the total uncertainty derived from the uncertainty of the
 1135 spike calibration (see subsection 2.3.2). Error bars are often smaller than the symbol size. The analytical
 1136 uncertainties for the literature data are not shown. The chondrite isochron is from Bouvier *et al.* (2008).



1137
 1138
 1139
 1140

1141 **Fig. 6.** Comparison of Rb and Sr abundances normalized by the mean Na and Al abundances, as a measure
 1142 for the amount of feldspar in the sample. The plotted groups are divided based on their weathering index.
 1143 The values for Non-Antarctic HC (Lit.) and Antarctic HC (Lit.) are calculated from Wasson and Kallemeyn
 1144 (1988), Jarosewich (1990), and Nishikawa *et al.* (1990), shown in Table 5. The uncertainties are derived from
 1145 the individual uncertainties of each elemental abundance, and those for literature values are 95% confidence
 1146 interval of the mean values. Error bars are often smaller than the symbol size.



1147

1148

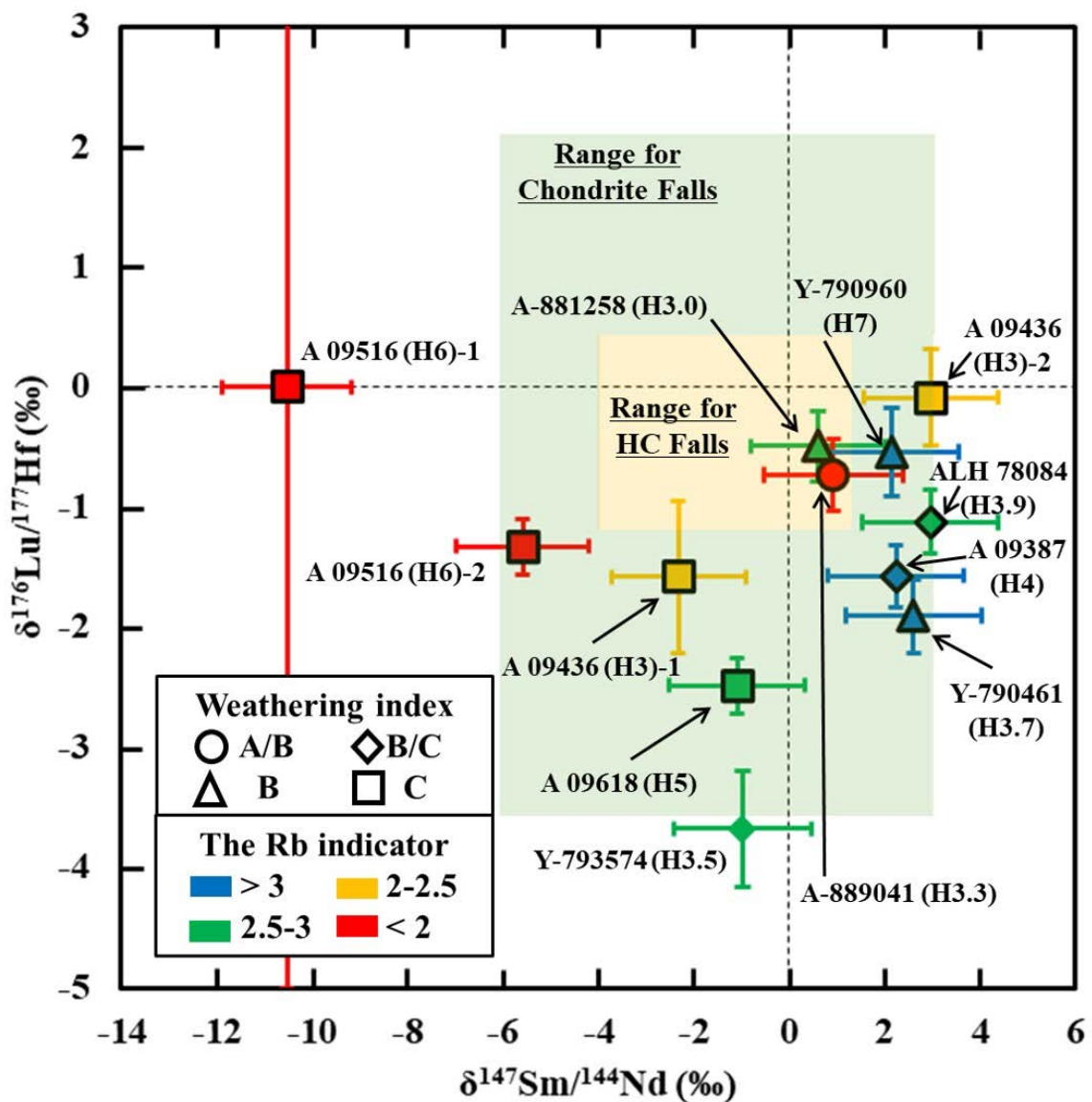
1149

1150

1151

1152

1153 **Fig. 7.** Deviations of $^{147}\text{Sm}/^{144}\text{Nd}$ and $^{176}\text{Lu}/^{177}\text{Hf}$ from the respective chondrite isochron on Sm-Nd and Lu-
 1154 Hf systems. The symbols of each plot reflect the weathering index and the Rb indicator (Table 5) by shape and color, respectively. Note that no weathering index for Y-793574 (H3.5) and $^{176}\text{Lu}/^{177}\text{Hf}$ of A 09516 (H6)-
 1155 1 have been determined, hence the symbol of Y-793574 (H3.5) is not surrounded by black line and the
 1156 $\delta^{176}\text{Lu}/^{177}\text{Hf}$ of A 09516 (H6)-1 was not determined. The ranges for chondrite falls and HC falls are calculated
 1157 from the literature values shown in Figs. 4 and 5 (Supplemental data), and are shown by light green and light
 1158 red, respectively. The respective isochrons used for the calculations are from Bouvier *et al.* (2008). The
 1159 uncertainties except for the $\delta^{176}\text{Lu}/^{177}\text{Hf}$ of A 09516 (H6)-1 are derived from the uncertainties of each
 1160 isotopic ratios. The uncertainties of the isochrons are not considered.
 1161



1162

1163

1164 **SUPPLEMENTARY DATA**

1165 **Supplementary data-1.** Sm-Nd and Lu-Hf isotopic compositions of H chondrite falls, chondrite falls, and Antarctic chondrites (WI: weathering index for Antarctic chondrites).

1166 The weathering indexes for Antarctic chondrites are from Antarctic Meteorite Newsletter, NASA. The chondrite fall mean includes H chondrites.

1167 *MAC 88136 and MAC 88180 are possibly paired (Antarctic Meteorite Newsletter 13, NASA).

1168 ^a Jacobsen and Wasserburg (1980). ^b Jacobsen and Wasserburg (1984). ^c Blichert-Toft and Albarède (1997). ^d Bizzarro *et al.* (2003). ^e Patchett *et al.* (2004). ^f Boyet and Carlson (2005). ^g Carlson *et al.*

1169 (2007). ^h Bouvier *et al.* (2008). ⁱ Dauphas and Pourmand (2011). ^j Gannoun *et al.* (2011). ^k Burkhardt *et al.* (2016). ^l Fukai and Yokoyama (2017).

1170 **Supplementary data-2.** Average Sm-Nd and Lu-Hf isotope compositions in each class calculated using only falls from the supplementary data-1.

1171 The uncertainties associated with the isotopic ratios are simply calculated at 2SE, except for $N = 2$, where the values reflect the range of values. Tieschitz and Bjurböle are excluded from this calculation

1172 due to their intermediate petrologic features. The following samples are excluded from the respective means because their values seem not to be representative: Farmington from Dauphas and Purmand

1173 (2011), M'Bale from Bizzarro *et al.* (2003), and Peace River from Carlson *et al.* (2007) for the means of L chondrites; Paragould from Dauphas and Purmand (2011) and Saint-Séverin (Light) and

1174 (Dark) from Jacobsen and Wasserburg (1980) for the means of LL chondrites; Orgueil from Blichert-Toft and Albarède (1997) for the means of CI chondrites; the Sm-Nd values of Alende piece from

1175 Patchett *et al.* (2004) and Grosnaja from Carlson *et al.* (2007) for the means of CV chondrites; Abee and Abee (bis) from Burkhardt *et al.* (2016) and Adhi Kot, St. Mark's, and Saint-Sauveur from

1176 Dauphas and Purmand (2011) for the means of EH chondrites; Eagle, Jajh Deh Kot Lulu, and Khairpur from Dauphas and Purmand (2011) for the means of EL chondrites.

1177

1178

Sm-Nd and Lu-Hf isotope compositions of H chondrite falls, chondrite falls, and Antarctic chondrites (WI: weathering index for Antarctic chondrites).

Meteorite	Class	Nd (ppb)	Sm (ppb)	¹⁴⁷ Sm/ ¹⁴⁴ Nd	2SE	¹⁴³ Nd/ ¹⁴⁴ Nd	2SE	Lu (ppb)	Hf (ppb)	¹⁷⁶ Lu/ ¹⁷⁷ Hf	2SE	¹⁷⁶ Hf/ ¹⁷⁷ Hf	2SE	Ref.
<u>H chondrite Falls</u>														
Sharps	H3.4	572	186	0,1959	0,0002	0,512624	0,000006							f
Sharps (bis)	H3.4	592	190	0,1951	0,0002	0,512622	0,000002							f
Sharps	H3.4	570	185	0,1963	0,0010	0,512644	0,000009	33,6	143	0,0334	0,0002	0,282791	0,000007	h
Dhajala	H3.8	623	201	0,1954	0,0002	0,512621	0,000003							f
Dhajala	H3.8	576	186	0,1958	0,0010	0,512633	0,000008	33,2	143	0,0330	0,0002	0,282740	0,000006	h
Ankober	H4	541	175	0,1960	0,0004	0,512604	0,000006	30,7	137	0,0317	0,0002	0,282661	0,000008	e
Avanhandava	H4	562	182	0,1961	0,0004	0,512617	0,000005	32,8	144	0,0324	0,0002	0,282669	0,000018	e
Bielokrynitschie	H4							31,4	144	0,0310	0,0004	0,282581	0,000036	i
Ochansk	H4	491	158	0,1941	0,0004	0,512638	0,000006	31,6	149	0,0301	0,0002	0,282444	0,000009	e
Ochansk (bis)	H4	618	200	0,1960	0,0004	0,512630	0,000009	35,3	150	0,0334	0,0002	0,282761	0,000016	e
Ochansk	H4							34,0	151	0,0320	0,0004	0,282699	0,000036	i

Kesen	H4							32,4	133	0,0348	0,0004	0,282849	0,000036	i
Sainte Marguerite	H4	702	227	0,1955	0,0002	0,512635	0,000006							k
Sainte Marguerite (bis)	H4	773	250	0,1954	0,0002	0,512636	0,000005							k
Allegan	H5	570	185	0,1958	0,0004	0,512646	0,000010	32,1	129	0,0352	0,0002	0,282951	0,000014	e
Allegan	H5	584	188	0,1952	0,0002	0,512615	0,000003							k
Forest City	H5	624	203	0,1964	0,0004	0,512634	0,000006	35,8	151	0,0336	0,0002	0,282782	0,000012	e
Forest City	H5	675	217	0,1944	0,0002	0,512599	0,000003							k
Forest City	H5			0,1960	0,0030	0,512633	0,000003							l
Gao	H5							33,2	141	0,0335	0,0003	0,282884	0,000020	c
Herredia	H5							32,4	143	0,0321	0,0003	0,282681	0,000037	c
Herredia	H5							34,3	143	0,0341	0,0001	0,282821	0,000022	d
Jilin	H5	550	173	0,1904		0,512581	0,000003							j
Pultusk	H5	592	193	0,1973	0,0004	0,512663	0,000006	35,1	148	0,0337	0,0002	0,282810	0,000014	e
Pultusk	H5	660	211	0,1934	0,0002	0,512608	0,000005							k
Richardton	H5	562	184	0,1979	0,0004	0,512648	0,000006	33,3	153	0,0310	0,0002	0,282593	0,000009	e
Richardton	H5	595	191	0,1942	0,0002	0,512622	0,000003							f
Guareña	H6	902	290	0,1947	0,0002	0,512560	0,000024							a
Kernouve	H6							29,3	129	0,0324	0,0004	0,282695	0,000036	i
Queens Mercy	H6	587	189	0,1946	0,0002	0,512597	0,000003							k
Ucera	H	569	185	0,1963		0,512645	0,000001							g
HC fall mean		613	198	0,1953	0,0006	0,512623	0,000009	33,0	143	0,0328	0,0007	0,282730	0,000060	
<i>N for the mean values</i>		<i>23</i>				<i>24</i>			<i>17</i>			<i>17</i>		

Chondrite Falls

Tieschitz	H/L3.4	633	203	0,1937	0,0010	0,512628	0,000007	36,0	157	0,0325	0,0002	0,282766	0,000006	h
Hallingeberg	L3.4	616	200	0,1960	0,0010	0,512629	0,000007	35,1	148	0,0336	0,0002	0,282781	0,000007	h
Hedjaz	L3.7							32,6	141	0,0329	0,0001	0,282726	0,000021	d
Mezo-Madaras	L3.7	621	201	0,1960	0,0010	0,512626	0,000009	35,6	152	0,0333	0,0002	0,282764	0,000004	h
Bovedy	L3.8	687	223	0,1961	0,0010	0,512629	0,000007	40,3	172	0,0333	0,0002	0,282657	0,000009	h

Bald Mountain	L4							37,1	147	0,0360	0,0004	0,283005	0,000036	i
Saratov	L4			0,1960	0,0002	0,512616	0,000005							l
Tennasilm	L4							36,6	154	0,0337	0,0003	0,282606	0,000025	c
Tennasilm	L4							33,8	146	0,0329	0,0001	0,282720	0,000025	d
Farmington	L5							44,2	148	0,0425	0,0004	0,283741	0,000036	i
Farmington	L5	655	210	0,1944	0,0002	0,512591	0,000006							k
Homestead	L5	678	218	0,1949	0,0004	0,512640	0,000008	35,2	150	0,0332	0,0002	0,282810	0,000009	e
Homestead	L5	583	188	0,1951		0,512625	0,000001							g
Alfianello	L6							33,5	155	0,0317		0,282599	0,000014	c
Alfianello	L6							42,3	169	0,0355	0,0001	0,282982	0,000013	d
Bruderheim	L6	530	173	0,1970	0,0004	0,512648	0,000006	31,0	145	0,0302	0,0002	0,282518	0,000022	e
Bruderheim	L6	540	175	0,1955	0,0004	0,512620	0,000003							f
Bruderheim	L6	909	291	0,1935	0,0002	0,512563	0,000003							k
Fisher	L6							37,1	150	0,0350	0,0004	0,282959	0,000008	c
Girgenti	L6	674	218	0,1954	0,0004	0,512643	0,000006	38,2	173	0,0313	0,0002	0,282597	0,000009	e
Harleton	L6							32,0	150	0,0303	0,0004	0,282421	0,000036	i
Holbrook	L6	557	182	0,1975	0,0004	0,512656	0,000008	33,9	159	0,0303	0,0002	0,282483	0,000012	e
Holbrook (bis)	L6	571	187	0,1974	0,0004	0,512677	0,000009	34,0	160	0,0301	0,0002	0,282544	0,000014	e
Leedey	L6			0,1966	0,0004	0,512629	0,000023							b
M'Bale	L6							35,4	152	0,0331	0,0003	0,282700	0,000016	c
M'Bale	L6							30,2	162	0,0264	0,0001	0,282127	0,000011	d
M'Bale (bis)	L6							36,8	171	0,0306	0,0001	0,282552	0,000025	d
Modoc (1905)	L6			0,1950	0,0020	0,512510	0,000005							l
Peace River	L6	606	82	0,1903		0,512641	0,000001							g
Bjurböle	L/LL4	650	208	0,1933	0,0004	0,512602	0,000007	38,9	170	0,0324	0,0002	0,282714	0,000008	e
Semarkona	LL3.0	662	215	0,1960	0,0010	0,512622	0,000012	37,8	162	0,0331	0,0002	0,282749	0,000005	h
Krymka	LL3.1	601	193	0,1945	0,0010	0,512575	0,000012	34,2	144	0,0337	0,0002	0,282786	0,000008	h
Chainpur	LL3.5	633	205	0,1956	0,0010	0,512623	0,000008	36,1	154	0,0333	0,0002	0,282786	0,000005	h
Parnallee	LL3.6	648	210	0,1961	0,0010	0,512622	0,000010	37,1	156	0,0339	0,0002	0,282809	0,000005	h

Hamlet	LL4							39,0	177	0,0314	0,0004	0,282619	0,000036	i
Soko-Banja	LL4							33,8	149	0,0324	0,0004	0,282722	0,000036	i
Chelyabinsk	LL5	661	215	0,1963	0,0002	0,512647	0,000003							k
Tuxtuac	LL5							38,9	168	0,0329	0,0004	0,282619	0,000036	i
Tuxtuac	LL5			0,1920	0,0020	0,512643	0,000005							l
Paragould	LL5							45,2	172	0,0375	0,0004	0,283217	0,000036	i
Dhurmsala	LL6	593	193	0,1965	0,0002	0,512637	0,000003							k
Saint-Séverin (Light)	LL6	1386	440	0,1920	0,0002	0,512464	0,000025							a
Saint-Séverin (Dark)	LL6	560	185	0,2000	0,0002	0,512735	0,000027							a
Saint-Séverin (WR)	LL6			0,1964	0,0002	0,512618	0,000020							b
Saint-Séverin	LL6							42,7	185	0,0330	0,0004	0,282735	0,000036	i
Saint-Séverin	LL6			0,1910	0,0020	0,512571	0,000007							l
Ivuna	CI1	410	133	0,1967	0,0010	0,512679	0,000013							h
Ivuna	CI1							28,0	116	0,0343	0,0004	0,282826	0,000036	i
Orgueil	CI1							27,4	130	0,0298	0,0003	0,282767	0,000033	c
Orgueil	CI1	462	150	0,1968		0,512639	0,000001							g
Orgueil	CI1	459	149	0,1964	0,0010	0,512609	0,000014	25,1	106	0,0335	0,0002	0,282784	0,000005	h
Cold Bokkeveld	CM2	602	195	0,1962		0,512639	0,000001							g
Mighei	CM2	612	199	0,1966	0,0004	0,512644	0,000006	35,0	147	0,0339	0,0002	0,282798	0,000007	e
Mighei	CM2	625	202	0,1953		0,512618	0,000001							g
Mighei	CM2							33,0	139	0,0338	0,0004	0,282795	0,000036	i
Murchison	CM2	635	207	0,1969	0,0002	0,512607	0,000025							a
Murchison (bis)	CM2	670	214	0,1932	0,0002	0,512529	0,000034							a
Murchison (ter)	CM2	643	209	0,1966	0,0002	0,512628	0,000025							a
Murchison	CM2			0,1966	0,0002	0,512627	0,000016							b
Murchison	CM2							30,8	129	0,0340	0,0003	0,282899	0,000035	c
Murchison	CM2							34,0	150	0,0323	0,0001	0,282679	0,000019	d
Murchison	CM2	632	207	0,1977	0,0004	0,512626	0,000008	35,6	150	0,0338	0,0002	0,282804	0,000010	e
Murchison	CM2			0,1970	0,0020	0,512613	0,000005							l

Murray	CM2	641	207	0,1949	0,0004	0,512632	0,000007	36,1	155	0,0330	0,0002	0,282742	0,000011	e
Murray	CM2	638	207	0,1962		0,512637	0,000001							g
Pollen	CM2			0,1967	0,0002	0,512641	0,000024							b
Al Rais	CR2	548	179	0,1970	0,0010	0,512647	0,000009							h
Felix	CO3.1	735	238	0,1959	0,0010	0,512620	0,000007	46,3	196	0,0335	0,0002	0,282777	0,000004	h
Kainsaz	CO3.2	727	237	0,1969	0,0004	0,512632	0,000006	59,9	242	0,0351	0,0002	0,282942	0,000006	e
Kainsaz	CO3.2							43,8	186	0,0335	0,0004	0,282817	0,000036	i
Lancé	CO3.5	733	239	0,1969	0,0010	0,512647	0,000014	40,5	169	0,0339	0,0002	0,282799	0,000004	h
Lancé	CO3.5							42,5	177	0,0333	0,0004	0,282762	0,000036	i
Bali	CV3.6	771	256	0,2006	0,0010	0,512763	0,000014	40,6	171	0,0338	0,0002	0,282838	0,000009	h
Allende	CV3.6	1020	327	0,1940	0,0010	0,512552	0,000006	45,6	191	0,0339	0,0002	0,282816	0,000018	h
Allende (bis)	CV3.6	1021	327	0,1939	0,0010	0,512559	0,000010	45,7	190	0,0340	0,0002	0,282824	0,000005	h
Allende	CV3							49,8	211	0,0335	0,0003	0,282776	0,000015	c
Allende (bis)	CV3							46,1	192	0,0341	0,0003	0,282825	0,000011	c
Allende	CV3							43,3	186	0,0331	0,0001	0,282783	0,000012	d
Alende piece	CV3	1319	406	0,1861	0,0004	0,512353	0,000007	42,4	177	0,0341	0,0002	0,282847	0,000007	e
Allende pdr	CV3	1010	325	0,1947	0,0004	0,512606	0,000009	49,6	206	0,0341	0,0002	0,282828	0,000017	e
Allende pdr (bis)	CV3	991	319	0,1947	0,0004	0,512589	0,000009	48,1	198	0,0344	0,0002	0,282834	0,000016	e
Allende	CV3	986	315	0,1930	0,0002	0,512573	0,000003							f
Allende (bis)	CV3	1010	324	0,1938	0,0002	0,512563	0,000002							f
Allende (ter)	CV3	980	313	0,1929	0,0002	0,512558	0,000003							f
Allende	CV3	854	275	0,1947		0,512566	0,000001							g
Allende	CV3							46,0	192	0,0341	0,0004	0,282835	0,000036	i
Allende (bis)	CV3							45,9	192	0,0341	0,0004	0,282795	0,000036	i
Allende (ter)	CV3							45,2	189	0,0340	0,0004	0,282839	0,000036	i
Allende (quarter)	CV3							48,5	206	0,0337	0,0004	0,282814	0,000036	i
Allende (quīnquiēs)	CV3							46,0	193	0,0340	0,0004	0,282824	0,000036	i
Allende (sexiēs)	CV3							46,4	193	0,0343	0,0004	0,282795	0,000036	i
Allende (septiēns)	CV3							46,1	192	0,0342	0,0004	0,282801	0,000036	i

Hvittis	EL6							30,4	134	0,0322	0,0004	0,282651	0,000036	i
Hvittis	EL6	361	120	0,2007		0,512750	0,000003							j
Hvittis	EL6	480	159	0,1999	0,0002	0,512758	0,000003							k
Hvittis (bis)	EL6	818	269	0,1986	0,0002	0,512753	0,000006							k
Hvittis (ter)	EL6	557	183	0,1993	0,0002	0,512766	0,000005							k
Jajh Deh Kot Lalu	EL6							22,9	159	0,0205	0,0004	0,281675	0,000036	i
Khairpur	EL6							24,1	137	0,0250	0,0004	0,282061	0,000036	i
Khairpur	EL6	411	134	0,1965		0,512633	0,000002							j
Pillistfer	EL6							26,8	119	0,0320	0,0003	0,282708	0,000014	c
Pillistfer	EL6							25,0	113	0,0316	0,0004	0,282648	0,000036	i
Chondrite fall mean				0,1955	0,0005	0,512622	0,000012			0,0331	0,0006	0,282757	0,000056	
N for the mean values						107						96		
<u>Antarctic chondrites</u>														
GRA 95229 (WI: A)	CR2							44,6	188	0,0336	0,0002	0,282787	0,000007	h
ALHA 77295 (WI: B)	EH3	344	114	0,2009		0,512607	0,000003							j
KLE 98300 (WI: A)	EH3	490	160	0,1976	0,0010	0,512668	0,000007	24,0	124	0,0273	0,0001	0,282208	0,000004	h
MAC 88136 (WI: A)*	EL3	397	127	0,1936	0,0010	0,512553	0,000008	29,0	122	0,0338	0,0002	0,282794	0,000007	h
MAC 88180 (WI: C)*	EL3	819	267	0,1974		0,512732	0,000003							j
MAC 02837 (WI: C)	EL3	497	163	0,1987		0,512653	0,000000							j
MAC 02839 (WI: C)	EL3	572	187	0,1976		0,512642	0,000003							j
Antarctic chondrite mean				0,1976	0,0019	0,512643	0,000049			0,0316	0,0043	0,282596	0,000388	
N for the mean values						6						3		

The weathering indexes for Antarctic chondrites are from Antarctic Meteorite Newsletter, NASA. The chondrite fall mean includes H chondrite falls.

*MAC 88136 and MAC 88180 are possibly paired (Antarctic Meteorite Newsletter 13, NASA).

^a Jacobsen and Wasserburg (1980). ^b Jacobsen and Wasserburg (1984). ^c Blichert-Toft and Albarède (1997). ^d Bizzarro *et al.* (2003). ^e Patchett *et al.* (2004). ^f Boyet and Carlson (2005). ^g Carlson *et al.* (2007). ^h Bouvier *et al.* (2008). ⁱ Dauphas and Pourmand (2011). ^j Gannoun *et al.* (2011). ^k Burkhardt *et al.* (2016). ^l Fukai and Yokoyama (2017).